

AD-771 616

TWO-DIMENSIONAL AIR CUSHION LANDING
SYSTEM PERIPHERAL JET CONFIGURATION
STUDY

John R. Rogers

Air Force Flight Dynamics Laboratory
Wright-Patterson Air Force Base, Ohio

September 1973

DISTRIBUTED BY:

NTIS

National Technical Information Service
U. S. DEPARTMENT OF COMMERCE
5285 Port Royal Road, Springfield Va. 22151

NOTICE

When Government drawings, specifications, or other data are used for any purpose other than in connection with a definitely related Government procurement operation, the United States Government thereby incurs no responsibility nor any obligation whatsoever; and the fact that the government may have formulated, furnished, or in any way supplied the said drawings, specifications, or other data, is not to be regarded by implication or otherwise as in any manner licensing the holder or any other person or corporation, or conveying any rights or permission to manufacture, use, or sell any patented invention that may in any way be related thereto.

ADDITIONAL	
NAME	Print Name <input type="checkbox"/>
NO	Ball Number <input type="checkbox"/>
DATE	<input type="checkbox"/>
Description	
BY	
DISTRIBUTION/AVAILABILITY CODES	
CLASS. CODE/SPECIAL	
A	

Copies of this report should not be returned unless return is required by security considerations, contractual obligations, or notice on a specific document.

Unclassified

AD 771616

Security Classification			DOCUMENT CONTROL DATA R & D	
(Security classification of title, body of abstract and indexing annotation must be entered when the overall report is classified)				
1. ORIGINATING ACTIVITY (Corporate author)		2a. REPORT SECURITY CLASSIFICATION		
Air Force Institute of Technology (AFIT-EN) Wright-Patterson AFB, Ohio 45433		Unclassified		
		2b. GROUP		
3. REPORT TITLE				
Two-Dimensional Air Cushion Landing System Peripheral Jet Configuration Study				
4. DESCRIPTIVE NOTES (Type of report and inclusive dates)				
AFIT Thesis				
5. AUTHOR(S) (First name, middle initial, last name)				
John R. Rogers Captain USAF				
6. REPORT DATE		7a. TOTAL NO. OF PAGES		7b. NO. OF PAGES
September 1973		98		6
8a. CONTRACT OR GRANT NO.		9a. ORIGINATOR'S REPORT NUMBER(S)		
b. PROJECT NO 13690202		AFFDL-TR-73-5		
c.		9b. OTHER REPORT NO(S) (Any other numbers that may be assigned this report)		
d.		GAM/AE/73-13		
10. DISTRIBUTION STATEMENT				
Approved for Public Release; Distribution Unlimited				
11. SUPPLEMENTARY NOTES		12. SPONSORING MILITARY ACTIVITY		
		Air Force Flight Dynamics Laboratory Wright-Patterson AFB, Ohio 45433		
13. ABSTRACT				
<p>A simplified two-dimensional peripheral jet theory for the equilibrium performance of an air cushion vehicle is investigated. The proposed theory intends to yield a rapid prediction of the actual flow rate and actual power requirements for an Air Cushion Landing System in the hover condition. Nine specific nozzle configurations were tested to determine which resulted in the best power-height performance and whether the theory is able to predict the experimental performance. Three single peripheral jet configurations were tested at a trunk pressure of 80 psfg. Six distributed jet configurations were tested at a trunk pressure of 40 psfg. Effects of inward flow injection angles of 30 degrees and 60 degrees were investigated.</p> <p>It was found that the simplified theory can adequately predict a value of the flow coefficient C_Q for an ACLS nozzle configuration. Values of the power-height parameter C_{pd} predicted by the theory always indicated better performance than was achieved experimentally. The beneficial effect of inward flow injection was demonstrated for each group of similar nozzle configurations. The single slot with 60 degree flow injection resulted in the best performance below cushion to trunk pressure ratios of 0.5. Above this pressure ratio the distributed jet configurations with 60 degree inward injection resulted in superior performance.</p>				
NATIONAL TECHNICAL INFORMATION SERVICE DTIC Report No. AD771616 Springfield, MA 01104				

DD FORM 1473

Unclassified

Security Classification

Unclassified

Security Classification

14 KEY WORDS	LINK A		LINK B		LINK C	
	ROLE	WT	ROLE	WT	ROLE	WT
Air Cushion Landing System						
Air Cushion Vehicles						
Aircraft Landing Gear						
Peripheral Jet Flow						
Hovercraft						
Ground Effect Machines						
Air Cushion Landing Gear						

Unclassified

**TWO-DIMENSIONAL AIR CUSHION LANDING
SYSTEM PERIPHERAL JET CONFIGURATION STUDY**

JOHN R. ROGERS, CAPTAIN, USAF

Approved for public release; distribution unlimited

1c

FOREWORD

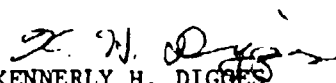
This work was conducted in support of an Air Force Flight Dynamics Laboratory in-house exploratory development effort on air cushion landing systems (Project 1369). The author conducted this work in partial fulfillment of the requirements for the degree of Master of Science from the Air Force Institute of Technology.

The author wishes to express his thanks to Dr. Andrew J. Shine, Prof. Harry R. Bulmer, and Dr. (Capt) J. T. Karam, Jr., his advisors, for their suggestions and advice.

The author is deeply indebted to the personnel of the AFIT Shop for their excellent workmanship. This undertaking would have been impossible without the technical assistance of Mr. David J. Pool and Mr. Shade Campbell of the Air Force Flight Dynamics Laboratory.

The author's special thanks go to Dr. Kennerly H. Digges, Chief, Mechanical Branch, Vehicle Equipment Division, Air Force Flight Dynamics Laboratory, for his suggestions and encouragement. Above all, the author would like to thank Dr. (Major) John C. Vaughan, III, Chief Scientist of the Mechanical Branch. His interest and encouragement made a potentially burdensome task quite an enjoyable and educational experience.

This technical report has been reviewed and is approved.


KENNERLY H. DIGGES
Chief, Mechanical Branch
Vehicle Equipment Division

ABSTRACT

A simplified two-dimensional peripheral jet theory for the equilibrium performance of an air cushion vehicle is investigated. The proposed theory intends to yield a rapid prediction of the actual flow rate and actual power requirements for an Air Cushion Landing System in the hover condition. Nine specific nozzle configurations were tested to determine which resulted in the best power-height performance and whether the theory is able to predict the experimental performance. Three single peripheral jet configurations were tested at a trunk pressure of 80 psfg. Six distributed jet configurations were tested at a trunk pressure of 40 psfg. Effects of inward flow injection angles of 30 degrees and 60 degrees were investigated.

It was found that the simplified theory can adequately predict a value of the flow coefficient C_Q for an ACLS nozzle configuration. Values of the power-height parameter C_{hd} predicted by the theory always indicated better performance than was achieved experimentally. The beneficial effect of inward flow injection was demonstrated for each group of similar nozzle configurations. The single slot with 60 degree flow injection resulted in the best performance below cushion to trunk pressure ratios of 0.5. Above this pressure ratio the distributed jet configurations with 60 degree inward injection resulted in superior performance.

CONTENTS

<u>Section</u>	<u>Page</u>
I. Introduction	1
Background	1
Air Cushion Landing System Problem Areas	3
Statement of the Problem	4
Objectives	8
Assumptions	8
Scope	9
II. Air Cushion Theory and Experimentation	10
Previous Theories	10
Previous Experimentation	11
Proposed Theory	11
III. Apparatus	15
Two-Dimensional Test Section	15
Air Supply	22
Ducting	22
Measuring Instruments	22

	<u>Page</u>
IV. Procedure	24
Leakage Test	24
Coefficient of Discharge Test	25
Nozzle Performance Test	26
V. Results	27
Flow Coefficient	27
Power-Height Parameter	29
VI. Conclusions and Recommendations	39
Conclusions	39
Recommendations	40
Bibliography	41
Appendix A: A Simplified Peripheral Jet Theory to Describe Equilibrium Hover Performance of an Air Cushion Vehicle	42
Appendix B: Derivation of Flow Rate Equations from the ASME Fluid Meters Report	48
Appendix C: Calculation of Test Section Leakage	55
Appendix D: Calculation of Nozzle Discharge Coefficients	60
Appendix E: Calculation of Nozzle Performance Parameters	66
Appendix F: Effective Flow Injection Angle Investigation	75
Appendix G: Effect of Outward Injection on Nozzle Flow Rate	77
Appendix H: Tabulated Theoretical and Experimental Data for the Flow Coefficient and Power-Height Parameter	79

LIST OF ILLUSTRATIONS

<u>Figure</u>	<u>Page</u>
1 Artist's Concept of a CC-115 Aircraft Configured with an air Cushion Landing System (ACLS)	2
2 General ACLS Model and Nomenclature	5
3 ACLS Distributed Jet Configuration	7
4 Theoretical Predictions of the Flow Coefficient	13
5 Theoretical Predictions of the Power-Height Parameter	14
6 Schematic of Experimental Apparatus	16
7 Test Section with Aluminum Trunk Installed	17
8 Aluminum Trunk Components	18
9 Representative Nozzle Configurations	21
10 Effect of Varying Pressure Ratio on Flow Coefficient	33
11 Variation of Power-Height Parameter with Cushion to Trunk Pressure Ratio	36
12 Model for Simplified Peripheral Jet Theory	47
13 Total Flow Rate Variation with Trunk Pressure	52
14 Fortran Program for the Calculation of Test Section Leakage	57
15 Test Section Leakage Variation with Trunk Pressure	59
16 Fortran Program for the Calculation of Nozzle Discharge Coefficients	63
17 Fortran Program for the Calculation of Nozzle Performance Parameters	69

<u>Table</u>	<u>Page</u>
I Nozzle Configuration Specifications	20
II f Values for Use in the Simplified Theory to Duplicate Experimental Flow Coefficient Results	32
III Nozzle Configuration Discharge Coefficients	62
IV Effective Nozzle Injection Angles	76
V Increase in Nozzle Flow Rate with Outward Injection	77
VI Theoretical and Experimental Values of the Flow Coefficient and Power-Height Parameter	80

LIST OF SYMBOLS

<u>Symbol</u>	<u>Description</u>	<u>Unit</u>
ACLS	Air Cushion Landing System	--
A_n	Nozzle exit area	in. ²
C_D	Nozzle coefficient of discharge	--
C_{hd}	Power-height parameter	--
C_Q	Nozzle flow coefficient, Q_n/Q_a	--
d	Daylight clearance (distance between trunk and surface)	in.
f	Nozzle to cushion pressure ratio, $(P_n - P_a) / (P_c - P_a)$	--
g_c	Dimensional constant	ft-lbm/lbf-sec ²
HP _{air}	Horsepower of airflow into trunk	hp
m	Mass flow rate of air	lbm/sec
P_a	Ambient pressure	psia
P_c	Cushion pressure	psia
P_t	Trunk pressure	psia
P_n	Nozzle exit pressure	psia

<u>Symbol</u>	<u>Description</u>	<u>Unit</u>
P_1	Upstream orifice pressure	psia
P_2	Downstream orifice pressure	psia
Q_a	Reference nozzle flow rate (at $P_c = P_a$)	cfs
Q_n	Actual nozzle flow rate (at any value of $P_c - P_a$)	cfs
R	Cushion to trunk pressure ratio ($P_c - P_a$) / ($P_t - P_a$)	--
S	Trunk perimeter (test section width for two-dimensional case)	ft.
t	Effective two-dimensional exit thickness of the trunk nozzles	in.
V_a	Reference average nozzle exit velocity (at $P_c = P_a$)	ft/sec
V_n	Actual average nozzle exit velocity	ft/sec
θ	Inward injection angle of trunk nozzles	degrees
ρ	Density	lbm/ft ³

Subscripts

exp	Experimental value
thy	Theoretical value

TWO-DIMENSIONAL AIR CUSHION LANDING SYSTEM

PERIPHERAL JET CONFIGURATION STUDY

I. Introduction

Background

The Air Force Flight Dynamics Laboratory is investigating the concept of an Air Cushion Landing System (ACLS). The system would consist of a torus-shaped membrane on the underside of an aircraft and an air source to provide the air flow necessary to inflate the membrane and support the aircraft a small distance above the ground. The membrane, called the trunk, would be inflated for takeoff, landing, and ground operations. Figure 1 is an artist's concept of a CC-115 aircraft configured with an ACLS. The trunk would be perforated with holes or slots to allow air to pass from the interior of the trunk to the area of lower pressure exterior to the trunk. When the aircraft approaches the ground this escaping air creates a region of pressure greater than ambient within the confines of the trunk underneath the aircraft. This area is called the cushion. The combined forces of the escaping air and the cushion pressure acting on the bottom of the fuselage support the aircraft a slight distance above the ground. This distance is called the daylight clearance, or jet height.

Interest in the ACLS has been stimulated by the success of several ground effect machines, air cushion vehicles, and hovercraft systems. Most of these vehicles operate primarily over water surfaces.

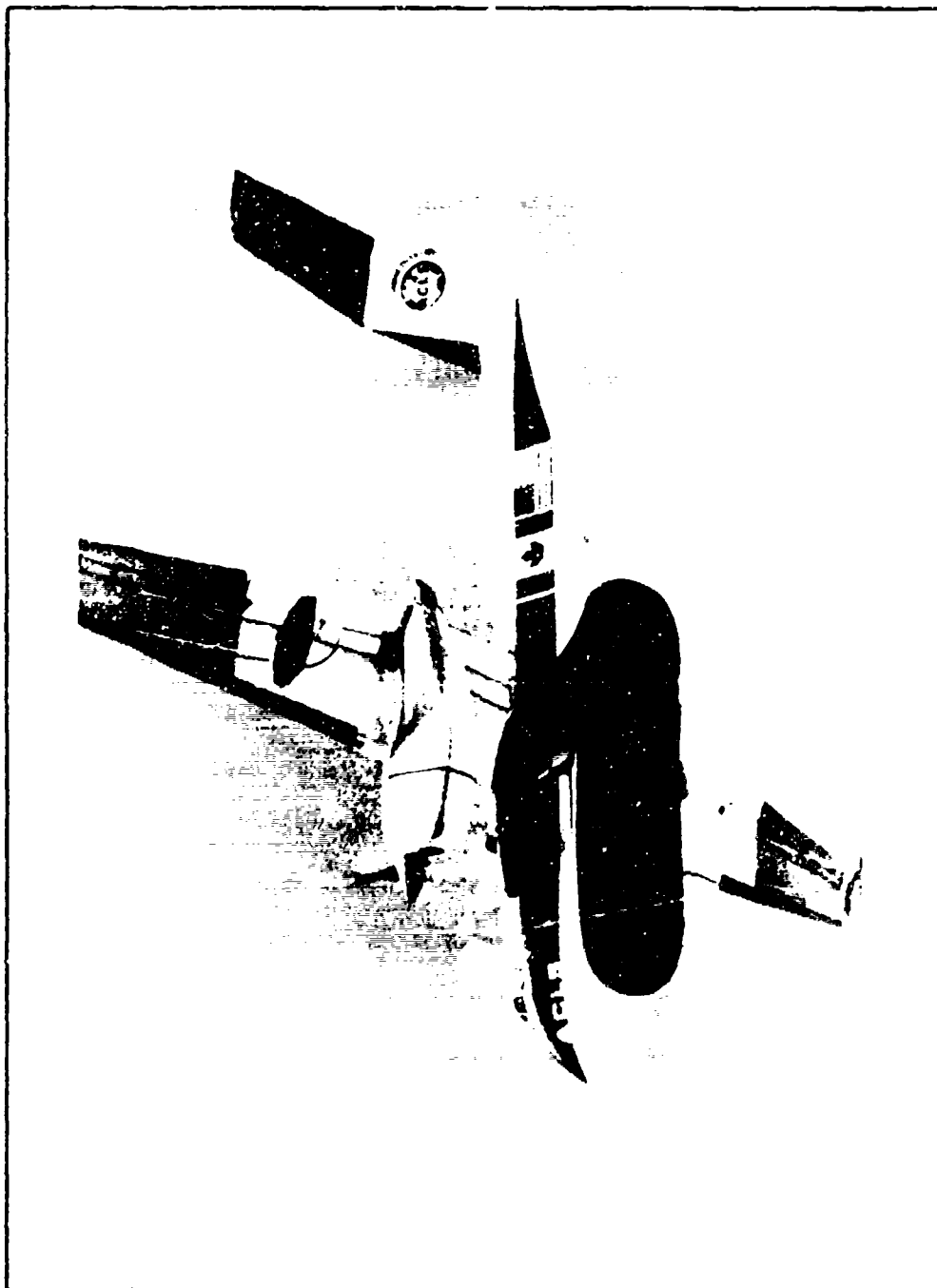


Fig. 1. Artist's Concept of a CC-115 Aircraft Configured with
an Air Cushion Landing System (ACLS)

Application of the concept to aircraft is appealing because an ACLS would permit operation from surfaces whose austerity prohibits the use of conventional landing gear. Much effort has been expended to improve the rough-field capabilities of conventional landing gear systems. To date, however, few of the conventional systems have proven to be reliable or efficient from unprepared surfaces.

Air Cushion Landing System Problem Areas

There are several problem areas associated with the development of a successful ACLS. One of the major problems is the selection of a suitable material for the trunk. The desired material is one that is flexible enough to allow inflation and complete deflation (i.e., stowage against the fuselage). On the other hand, the material must be durable enough to withstand the force and wear which occurs during ground operations.

A host of other problems must also be addressed. An effective braking system must be developed. An efficient method of attaching the trunk to the fuselage must be found. Attention must also be directed to the maintenance and logistical problems which will exist when the ACLS becomes operational. The final design should lend itself to relatively simple, rapid maintenance. Redundancies must be designed into the system. One laceration in the trunk should not render the entire system inoperative. Likewise, some thought should be given to the problem of partial or complete failure of the power source which inflates the trunk. Conventional landing gears afford some protection even with a partial failure such as a blown tire. The failure of one component

of the ACLS should not result in complete failure, possibly causing substantial structural damage to a landing aircraft.

Static and dynamic stability and control of the system must be investigated. How will the system behave during onload and offload of cargo? If applied to fighter type aircraft, will it affect munitions carrying capability? Will the system cause a foreign object ingestion problem for the engines? How noisy will the system be? How will the aircraft be parked when all power is removed? In the final analysis, will an aircraft configured with an ACLS provide sufficiently improved performance and/or capabilities which will justify the development costs?

These are among some of the fundamental issues which must be addressed before an ACLS is operationally feasible. Perhaps the most immediate problem, however, is determining the power which will be required to provide sufficient air flow to the trunk in order to yield the desired clearance of the aircraft above the ground during hover. Determination of the power requirement will dictate the type, size, and cost of the power source(s). It will also give an estimate of the weight to be incurred and the ducting required. This study is concerned with an aspect of the determination of the power requirement for an ACLS configuration in the hover condition.

Statement of the Problem

Figure 2 presents a general model of an ACLS and much of the associated nomenclature. This model depicts a trunk with one slot

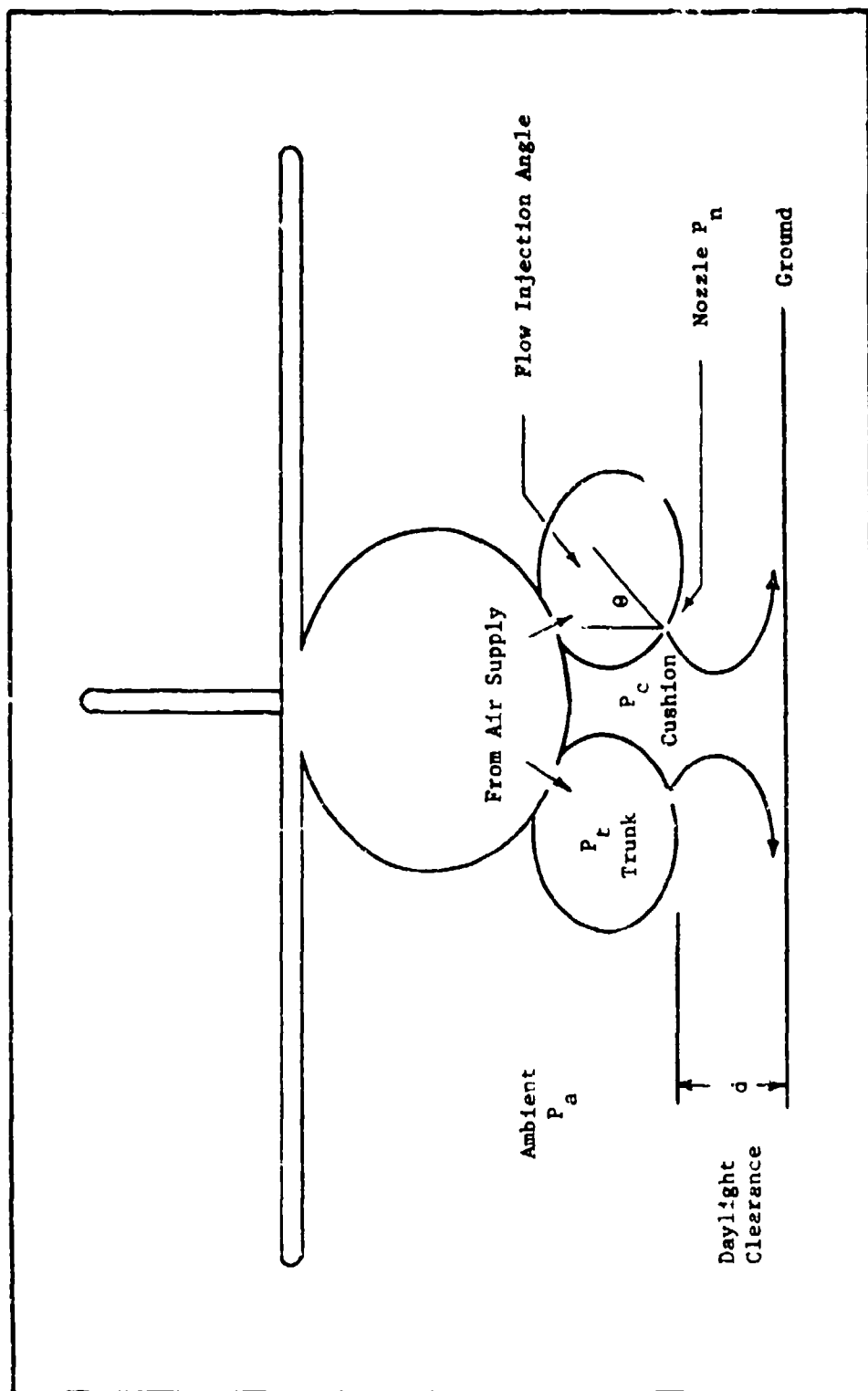
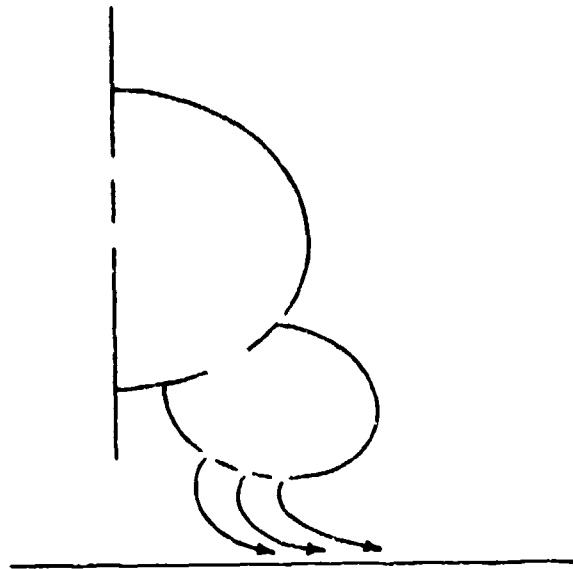


Fig. 2. General ACLS Model and Nomenclature

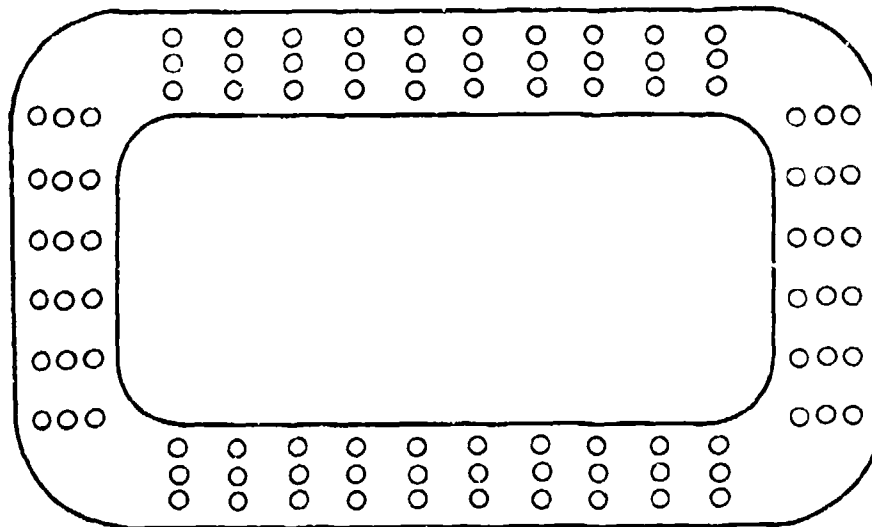
(peripheral jet) which extends, theoretically, around the entire perimeter of the trunk. Such a nozzle configuration is called a single peripheral jet. An actual ACLS will have multiple slots or rows of holes in the trunk, as shown in Figure 3. This is termed a distributed jet configuration. Analysis of the power requirements of an ACLS proceeds by applying the principles of conservation of mass, momentum, and energy to a control volume about the nozzle configuration of the model.

Several theories have been advanced for the estimation of the static and/or dynamic performance of an ACLS. Some of these will be discussed in further detail in Chapter II. Two non-dimensional parameters have proven to be of significance in evaluating the static performance of an ACLS. The first is a power-height parameter C_{hd} introduced by Digges (Ref 3). This parameter serves as a measure of the power required to yield a desired height of the vehicle above the ground. The second useful parameter is a flow coefficient C_Q . This parameter reflects the change in the nozzle flow rate caused by varying the ratio of cushion pressure to trunk pressure.

All of the previously developed momentum theories result in an expression for C_Q . Digges' expression for C_{hd} may be written directly in terms of C_Q . Thus values of C_Q and C_{hd} may be computed from any of the previous momentum theories. However, the expressions are generally quite involved mathematically, and a feel for the physical problem is lost. Also, only two of the previous theories have been shown to agree closely with experiment.



a. Vertical Section Showing a Distributed Jet Configuration



b. Bottom View of a Distributed Jet Configuration

Fig. 3. ACLS Distributed Jet Configuration

This study will be primarily concerned with a simplified jet theory developed by Major John C. Vaughan of the Air Force Flight Dynamics Laboratory. His theory also results in expressions for C_Q and C_{hd} for the hover condition. The pertinent portions of Vaughan's theory are presented in Appendix A.

Objectives. The two objectives of this study are: (1) to perform experimental work to evaluate the usefulness of the expressions for C_Q and C_{hd} developed in the simplified jet theory, and (2) to test nine specific two-dimensional nozzle configurations to determine which results in the best power-height performance (the lowest experimental value of C_{hd}).

Assumptions. For the purpose of initiating the study it is assumed that the model for Vaughan's simplified jet theory (see Fig. 12) is a realistic representation of the physical situation. The degree to which the experimental apparatus used in this study satisfied the model and meets the assumptions made in the development of the theory must be considered.

The theory is restricted to an ACLS in equilibrium over a smooth, solid, horizontal surface. The one in. thick plywood floor of the test apparatus was maintained as close as possible to horizontal by use of the floor jacks and levels discussed in Chapter III.

The theory assumes no aerodynamic lift (no forward motion) and no contact between the vehicle and the ground. These conditions were satisfied since the trunk section is stationary and the floor was not allowed to touch the trunk.

Vaughan's theory assumes that the flow within the control volume is steady and incompressible. The flow was allowed to stabilize approximately five minutes at each condition before data was taken. At low trunk pressures the flow was very steady. At trunk pressures above 60 psfg the flow fluctuated slightly but did not prevent accurate measurement. The pressure difference across the nozzle configuration being tested was always low enough to keep the flow incompressible.

The last two assumptions made in the theory concern the nature of the flow. The first of these is that the jet issuing from the nozzle maintains a constant thickness within the control volume. The last assumption is that the pressure at the nozzle can be expressed as the sum of the ambient pressure plus some fraction of the cushion pressure. The fraction may depend on the particular nozzle configuration, the flow injection angle and the ratio of cushion pressure to trunk pressure.

Scope. The scope of this study is limited in several respects. The entire study, both the experimental work and the theory which it concerns, is two-dimensional in nature. The results will apply strictly for a hover condition, as the experimentation does not include dynamic effects. The effect of injecting a portion of the flow directly into the cushion region was not investigated.

II. Air Cushion Theory and Experimentation

Previous Theories

Several different flow theories have been developed by authors who made various assumptions and/or modifications regarding the general physical model shown in Fig. 2. Digges reviewed the development of four such inviscid momentum theories, using the appropriate models and assumptions. In his theory, Digges introduced a power-height parameter C_{hd} . The expression for C_{hd} involves all the physical variables in the power problem. Thus it serves as a good measure for the relative power requirements of competing nozzle configurations. In equation form, Digges' expression for C_{hd} is

$$C_{hd} = \frac{HP_{air}}{(144)(d)} \frac{550}{S} \frac{1}{(2g_c/\rho)^{1/2}} \frac{1}{(P_c - P_a)^{3/2}} \quad (1)$$

where $HP_{air} = \frac{(144)(P_t - P_a)(Q_n)}{(550)}$

It can be seen from equation 1 that a low value of C_{hd} is desirable. A good nozzle configuration is one which will maximize d for a given HP_{air} . Stated differently, a good nozzle configuration is one which requires the least HP_{air} to achieve a desired d . Digges also extended single peripheral jet theory to account for distributed jet configurations, which will be used in actual air cushion landing systems.

Previous Experimentation

Digges performed two-dimensional experimental work to determine the power requirements of two specific distributed jet configurations in a flexible trunk. The first configuration consisted of four 1/8 in. slots. The second consisted of 192 holes 5/16 in. in diameter in eight staggered rows of 24 holes each. Digges found that the slotted trunk gave better performance (lower experimental values of C_{hd}) for values of cushion to trunk pressure R less than approximately 0.6. The hole configuration proved superior at R values greater than 0.6.

Gorman (Ref 4) performed additional work with the hole configuration. Han (Ref 5) performed two-dimensional experimental work with multiple hole configurations. The configurations differed in porosity and spacing. Han was primarily interested in cushion pressure prediction; however, power-height performance can be calculated from his test data.

Proposed Theory

The benefit of Vaughan's simplified theory lies in the mathematical simplification it affords while maintaining a feel for the physical problem. The theory will allow the prediction of values for C_Q and C_{hd} if the value of a factor f can be assigned to a particular nozzle configuration operating at a given value of R . The factor f is the percentage of the cushion pressure which the nozzle exit "sees". Figure 5 shows the values of C_{hd} predicted by various theories for different values of R , the cushion to trunk pressure ratio. The Barratt and Exponential theories are two of the earlier momentum theories. The two remaining curves show C_{hd} values predicted by Vaughan's theory for f values of 0.50 and 0.85. This demonstrates the utility of the simplified theory.

If values of the factor f can be assigned to a nozzle configuration based on experiment, then a value of C_{hd} can be predicted directly from a figure such as Figure 5. The same can be done for the flow coefficient C_Q , as shown in Figure 4. Thus the use of the simplified theory with f values based on experiment will yield the same results as the more involved theories.

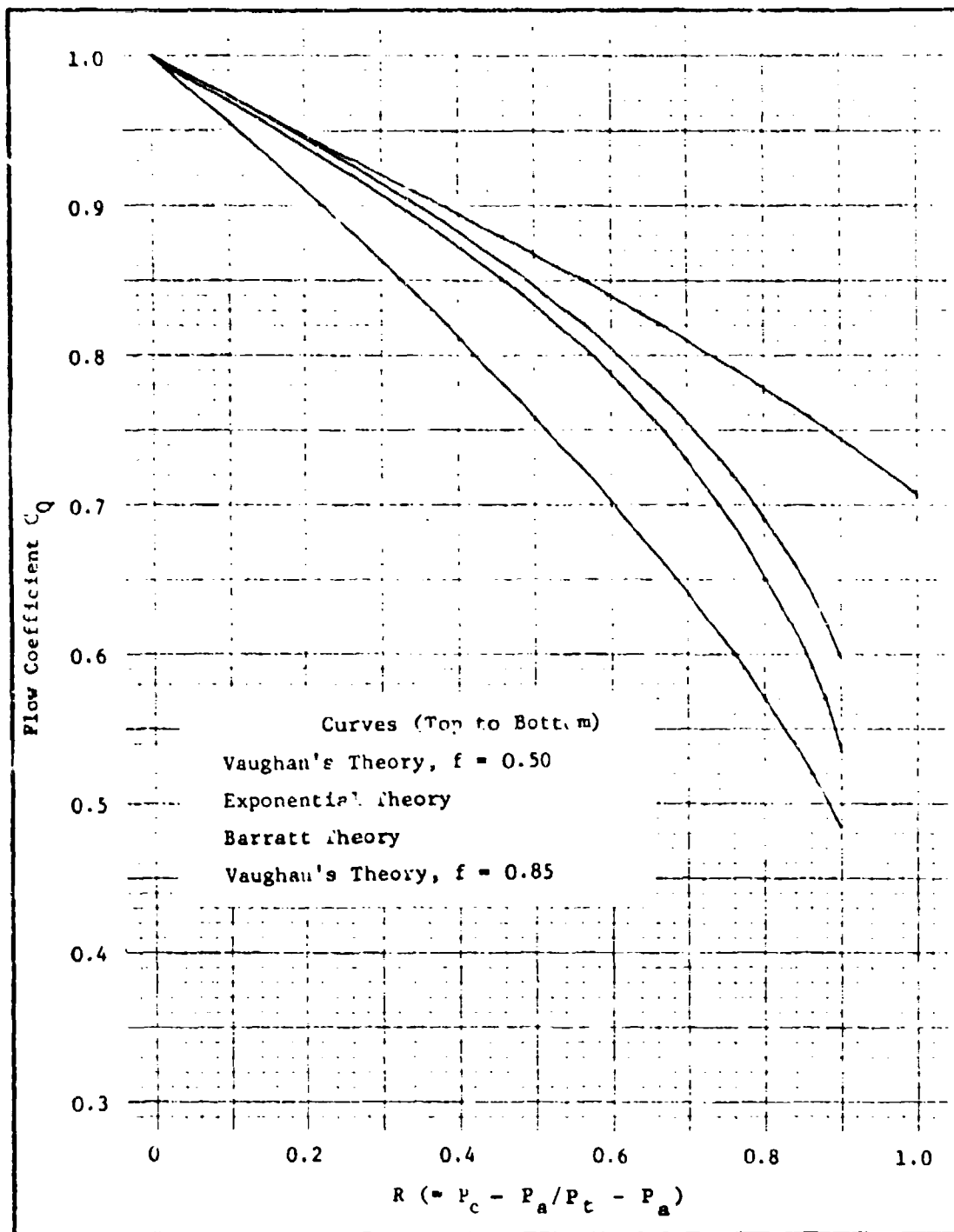


Fig. 4. Theoretical Predictions of the Flow Coefficient

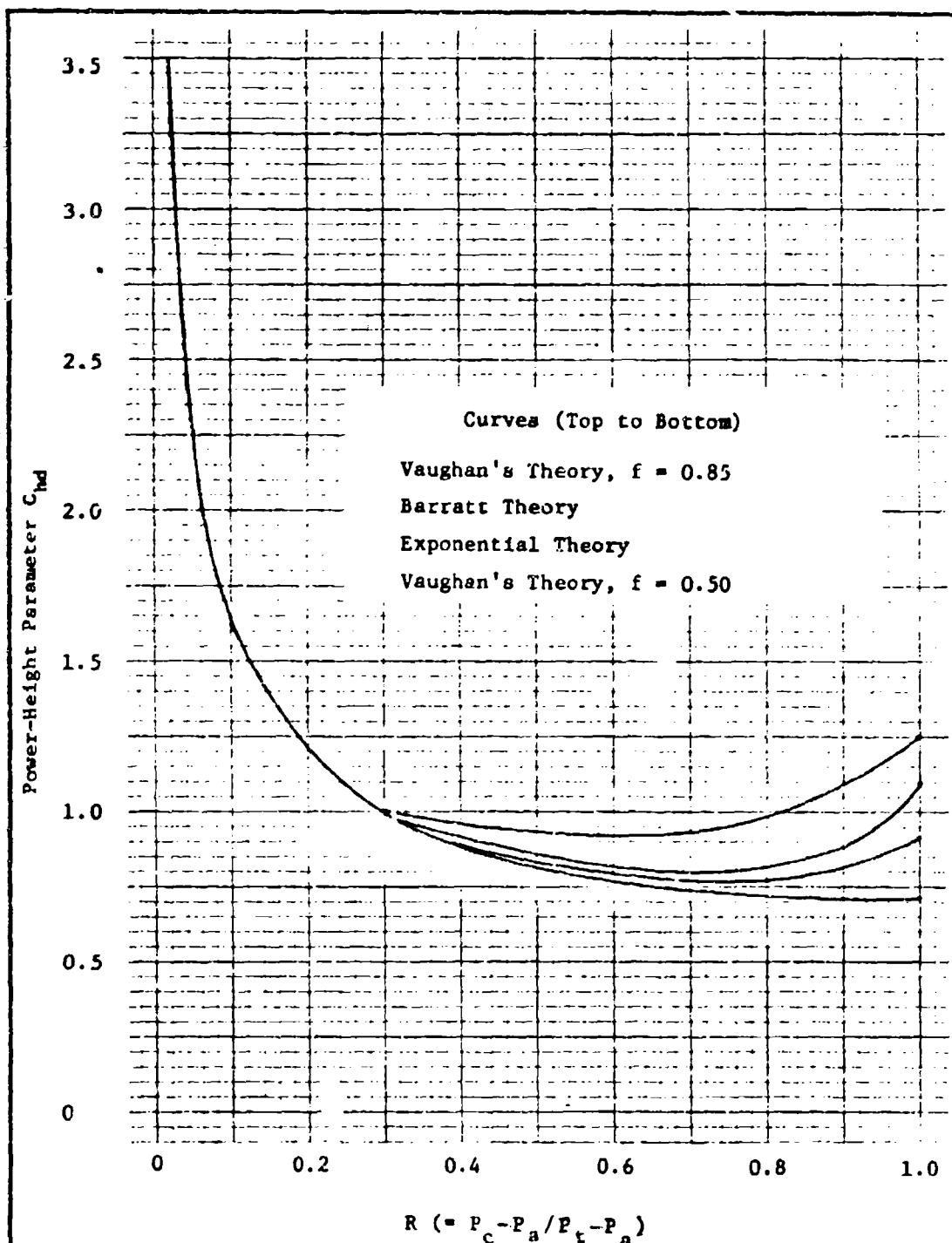


Fig. 5 Theoretical Predictions of the Power-Height Parameter

III. Apparatus

The test apparatus consisted primarily of an air supply, ducting, and a two-dimensional test section for the evaluation of the nine nozzle configurations. A schematic of the entire apparatus is shown in Fig. 6. Several instruments were used for the measurement of the pressures, distances and temperatures required for the calculation of air flow rates and nozzle performance parameters. The apparatus is essentially the same as that used by Digges and Gorman; however, it was fitted with an aluminum trunk section with changeable nozzle plates. Digges and Gorman had performed tests with a flexible trunk constructed of a nylon-hypalon material.

Two-Dimensional Test Section

The two-dimensional test section models the ACLS trunk, the cushion region and the ground plane. The major part of the box-like test section is made of one in. thick plywood. One wall is made of one in. thick plexiglass. In Fig. 7 the test section is shown with the aluminum trunk installed. The major components of the test section are the aluminum trunk, the floor assembly, and the floor jacks.

For the purposes of this study an aluminum trunk was used in lieu of the flexible trunk for two reasons. The first was the requirement for accurate measurement of the daylight clearance. The flexible trunk vibrated under certain loaded conditions and did not allow accurate

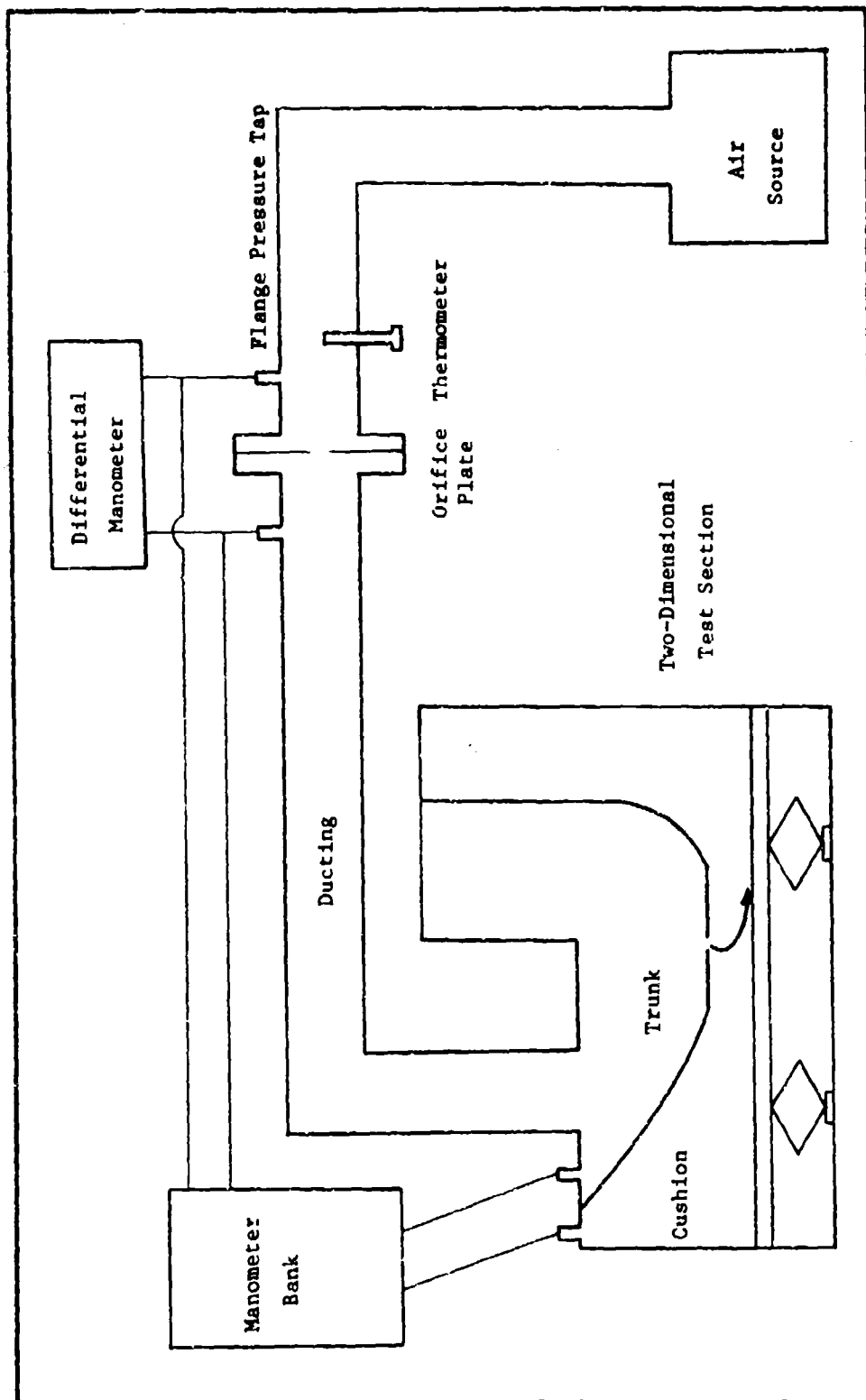


Fig. 6. Schematic of Experimental Apparatus

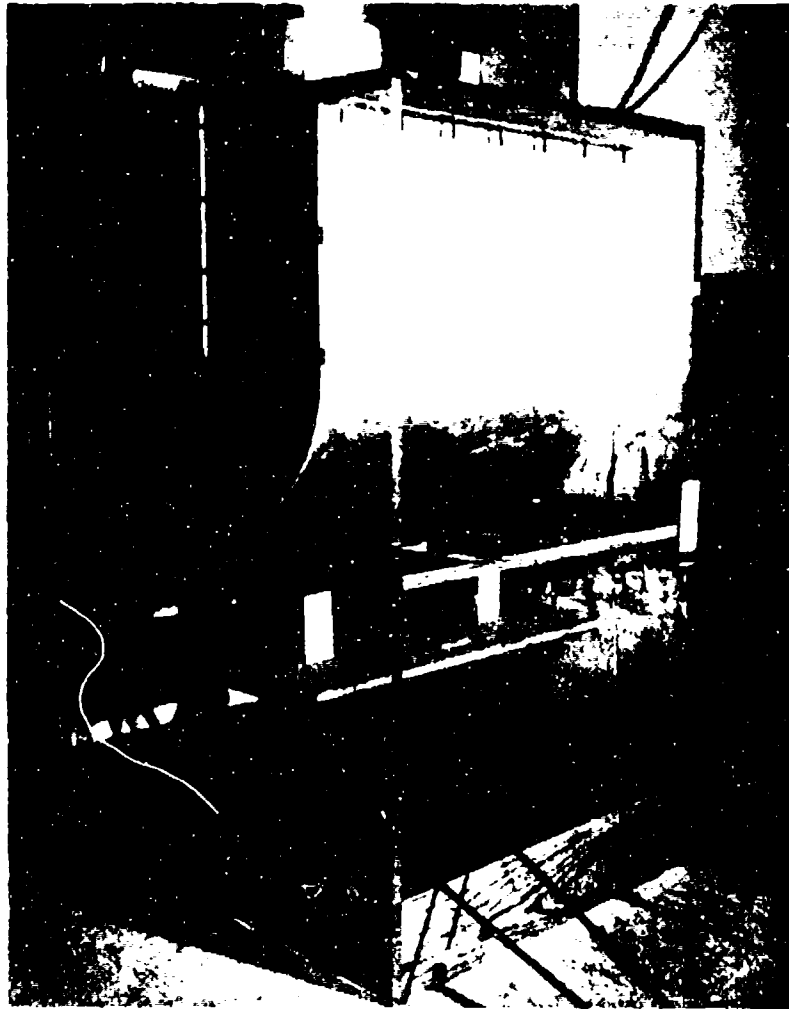


Fig. 7. Test Section with Aluminum Trunk Installed

measurement of the daylight clearance. The second reason for the aluminum trunk was that it allowed the testing of several different nozzle configurations using a common permanent trunk section. This obviated the construction of nine separate trunks. The aluminum trunk consists of the three sections shown in Fig. 8.

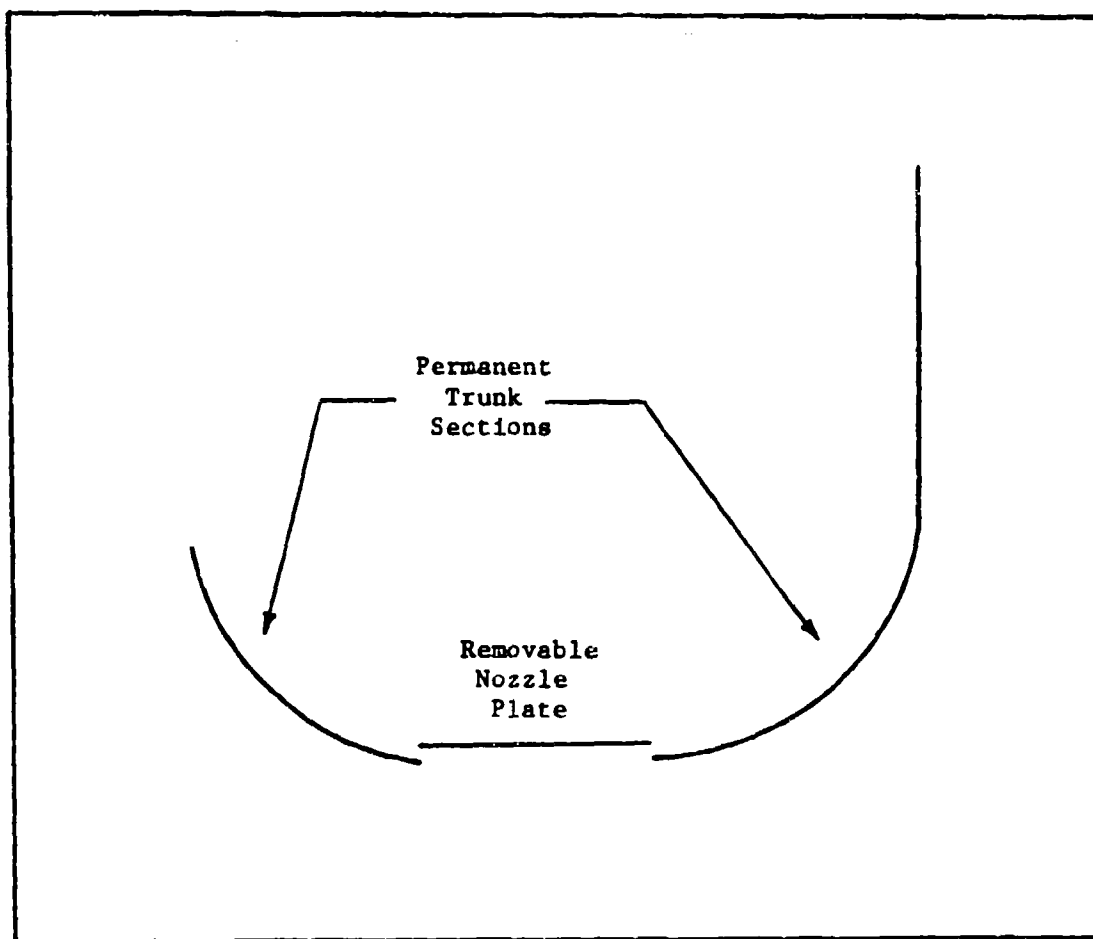


Fig. 8. Aluminum Trunk Components

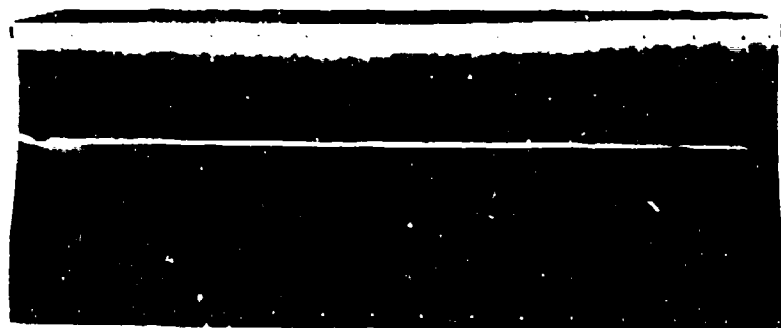
The curved portion of the trunk was rolled into the shape which the flexible trunk had assumed during previous tests for a cushion to trunk pressure ratio of 0.52 (Ref 3:179). The shape at this particular pressure ratio was chosen because such a hover pressure ratio has been used in the actual design of an ACLS for the CC-115 aircraft (Ref 1:7). The permanent sections are made of 1/8 in. thick aluminum. The details of the removable nozzle plates are given in Table I. After the permanent sections were installed a silicone rubber sealant was applied along the junction of the trunk and the walls of the test section. The nozzle plates were fastened into the permanent trunk sections for testing. Figure 9 illustrates one of each of the three types of nozzle configurations.

The floor assembly, used to simulate the ground plane, consisted of two pieces. The main floor was constructed of one in. thick plywood with a width of 32 in. and a depth of 42 in. The sub-floor was made with four legs extending upward to protect the pressure taps protruding from the bottom of the main floor.

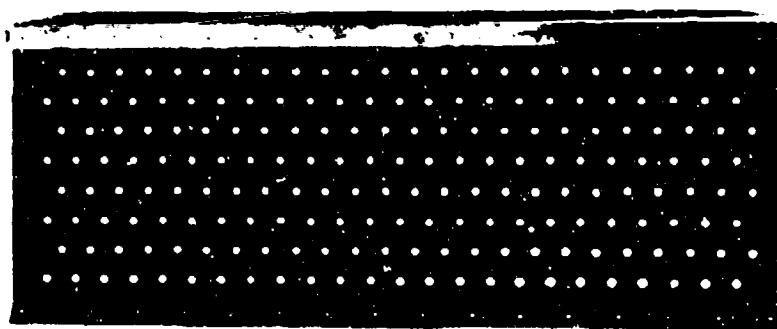
Four scissor-type automobile jacks were fastened to the bottom of the test section and were used to vary the height of the floor assembly to provide the required daylight clearance. The floor was leveled with the aid of bubble levels placed on two sides of the sub-floor. Horizontal strips of tape along the plexiglass wall of the test section also served as a level reference.

Config- uration	Single or Distributed Jet	Curved or Flat	Thickness (In.)	Arrangement	Size of Slots (Width) or Holes (Diam) (In.)	Total Nozzle Area ₂ (In. ²)	Injection Angle (Degrees)
21	Single	Curved	1/4	1 Slot	1/8	3.688	0
22	Single	Curved	1/4	1 Slot	1/8	3.750	30
23	Single	Curved	1/4	1 Slot	1/8	3.750	60
24	Distributed	Flat	1/8	8 Staggered Rows of 24 Holes Each	5/16	14.726	0
25	Distributed	Flat	1/4	8 Staggered Rows of 24 Holes Each	5/16	14.726	30
26	Distributed	Flat	1/4	8 Staggered Rows of 24 Holes Each	5/16	14.726	60
27	Distributed	Flat	1/4	4 Slots	1/8	14.270	0
28	Distributed	Flat	1/4	4 Slots	1/8	14.145	30
29	Distributed	Flat	1/4	4 Slots	1/8	13.773	60

Table I. Nozzle Configuration Specifications



a. Single Slot (Configurations 21, 22, 23)



b. 192 Holes (Configurations 24, 25, 26)



c. Four Slots (Configurations 27, 28, 29)

Fig. 9. Representative Nozzle Configurations

Air Supply

The air supply used for all tests was the same as that used by Digges and Gorman. The Spenser Gas Booster has a rated capacity of 3000 cfm at 1.65 psig. The airflow required to produce a desired trunk pressure was set by means of a butterfly valve located in the blower housing of the gas booster.

Ducting

Twelve in. diameter galvanized ducting connected the air supply and the test section. The horizontal portion of the duct was approximately sixteen feet long. The duct downstream of the orifice plate was sealed and taped prior to the first test.

Measuring Instruments

Measurement of flow rates, pressures, distances, and temperatures was required for the calculation of the nozzle performance parameters.

Measurement of the airflow rate to the test section was performed with the use of square-edged orifices constructed and mounted in accordance with the standards specified by the American Society of Mechanical Engineers (Ref 5:198). Two such orifices were constructed. A 2.4 in. diameter orifice was used for the leakage tests, during which low flow rates were encountered. A 3.6 in. diameter orifice was used for all of the tests which involved evaluation of the nozzle configurations. The appropriate orifice plate was bolted to flanges in the horizontal portion of the duct five feet upstream of the test section.

The pressures which required measurement during the tests were the trunk pressure, cushion pressure, upstream orifice pressure, and the downstream orifice pressure. These pressures were measured with four tubes of a 100 tube well manometer filled with water. Whenever possible the pressure differential across the orifice was also read from a U-tube differential manometer filled with water. When testing the large nozzle area configurations at the higher trunk pressures the differential pressure across the orifice exceeded the capability of the differential manometer. Both the well manometer and the differential manometer were calibrated in tenths of an in. of water. The trunk pressure was tapped in two places and fed to a Y-connector, which averaged their value. The same was done for the cushion pressure.

The daylight clearance, or distance between the floor and the trunk, was measured for all nozzle performance tests. This was accomplished with various size telescoping gauges and thickness gauges. The distance measured with the gauges was read using micrometers. Since the daylight clearance was not exactly constant across the width of the test section, the average of five measurements was used in the actual nozzle performance calculations.

Two 0-100 C thermometers were used for temperature measurement. One was located in the duct 10 in. upstream of the orifice plate. This temperature was used in the calculation of the total flow rates to the test section. The second thermometer was located inside the trunk in the vicinity of the nozzle plate. This temperature was used in the calculation of the nozzle flow rates.

IV. Procedure

Testing consisted of the three different types of tests discussed below.

Leakage Test

Prior to conducting the performance tests it was necessary to determine the leakage mass flow rate of the basic test section as a function of trunk pressure. This leakage rate was subtracted from the total measured mass flow rate in later tests before nozzle performance was determined.

For the leakage tests a solid plate was installed in the test section. All leakage tests were taken with cushion pressure equal to ambient, since there was no way to sustain a cushion pressure with a blank nozzle plate installed. Therefore, the values of leakage used in later performance calculations were pessimistic values, since less leakage would occur if the cushion pressure were higher than ambient.

Leakage tests were performed for trunk pressures from 10 psfg to 140 psfg in intervals of 10 psfg. Two series of leakage tests were performed. The first series was performed prior to all the nozzle tests; the second, after the completion of all nozzle tests. The linear approximation to the initial leakage tests, shown in Fig. 15, was used for the nozzle discharge coefficient and performance calculations.

The leakage rate was five percent of the total flow rate during tests of the single slot configurations. The leakage rate equalled two percent of the total flow rate during tests of the other six configurations.

An explanation of the leakage calculations is given in Appendix C.

Coefficient of Discharge Test

A coefficient of discharge was needed to determine the effective nozzle area of each nozzle configuration and trunk pressure combination to be used in the nozzle performance tests. Thus, a coefficient of discharge test was performed for each nozzle configuration prior to the nozzle performance tests. The only coefficient of discharge actually needed for each configuration was the one for the trunk pressure at which the nozzle performance tests were to be conducted. Nozzle performance tests for configurations 21, 22 and 23 were conducted at a trunk pressure of 80 psfg. The remaining configurations were tested at a trunk pressure of 40 psfg due to the limited airflow available for these large nozzle area configurations. Nevertheless, discharge coefficients were determined for configurations 21, 22 and 23 for trunk pressures from 10 psfg to 140 psfg in intervals of 10 psfg. Discharge coefficients for configurations 24 through 29 were determined for trunk pressures from 10 psfg to 50 psfg in intervals of 10 psfg. The values are given in Table III in Appendix D. The coefficient of discharge tests for each nozzle configuration were performed immediately prior to the nozzle performance tests in order to test under the same ambient conditions and the same orifice temperature conditions.

The floor assembly was removed for discharge coefficient tests to prevent the creation of a cushion pressure. Data was recorded for each desired trunk pressure.

An explanation of the coefficient of discharge calculations is given in Appendix D.

Nozzle Performance Test

The nozzle performance tests consisted of raising and lowering the floor assembly to create different ratios of gauge cushion pressure to gauge trunk pressure at a constant trunk pressure. The first test for each configuration was performed with the floor removed; that is, an R value of zero. The remainder of the tests for each nozzle were performed with the floor assembly in the test section. The first test with the floor installed was performed for an R value of approximately 0.10. The four scissor jacks and the flow rate were adjusted until the proper trunk pressure and R value existed simultaneously. This procedure was repeated for R values from 0.10 to 0.90 (or until the floor approached the trunk) in intervals of 0.10. Then the floor was lowered and the process repeated for R values from 0.85 (or from where the floor had approached the trunk) to 0.15 in decreasing intervals of 0.10.

An explanation of the nozzle performance calculations is given in Appendix E.

V. Results

To accomplish the first objective of the study (an evaluation of Vaughan's theoretical expressions for C_Q and C_{hd}), tests were performed with the nine nozzle configurations. The experimental value of the flow coefficient C_Q was computed as the ratio of the actual nozzle flow rate Q_n at any value of R to the reference nozzle flow rate Q_a (at $R = 0$). The experimental data points were plotted along with Vaughan's theoretical curves for $f = 0.50, 0.75$ and 1.00 . Experimental values of C_{hd} were determined with eq 1. Theoretical C_{hd} values were determined with eq 4, using the experimental C_Q values. The theoretical curves were plotted along with the experimental data points.

To accomplish the second objective of the study the experimental power-height performance of the nine nozzle configurations was compared to determine which was superior.

Flow Coefficient

The variation of the value of the flow coefficient C_Q with the cushion to trunk pressure ratio R is shown in Fig. 10. For actual ACLS operation, ranges of R between 0.40 and 0.70 are desired for stability reasons. Table II gives the values of f which, when used in Vaughan's theoretical expression for C_Q , would agree with the experimental results.

In the group of single slot nozzles (21, 22, 23) it is noted that the change in the flow injection angle has little or no effect on the resulting value of f , which remains near 0.90 for all the plates between $R = 0.40$ and $R = 0.70$. Thus f is not a function of either R or θ .

In the group of nozzles with 192 holes (24, 25, 26) both 30 degree and 60 degree flow injection produce the same considerable change in f value as compared to 0 degree injection. For the holes at 0 degrees the value of f varies from 0.50 (at $R = 0.40$) to 0.65 (at $R = 0.70$). For both the 30 degree holes and the 60 degree holes the value of f remains near 0.85 for all values of R between 0.40 and 0.70. Thus f is a function of R only for the 0 degree holes.

In the group of nozzles with four slots (27, 28, 29) the effect of increasing the flow injection angle is to broaden the range of f values exhibited. For the four slots at 0 degrees, f remains between 0.80 and 0.85 for R values from 0.40 to 0.70. For the four slots at 30 degrees, f varies from 0.70 to 0.85 for R values from 0.40 to 0.70, respectively. For the four slots at 60 degrees, f varies from 0.40 to 0.65 as R is varied from 0.40 to 0.70, respectively. For this series of plates f depends on both R and θ .

Thus the effect of varying the flow injection angle was not the same for all the configurations. In the first series of plates (single slot), varying the flow injection angle had almost no effect. In the second series of plates (192 holes) the difference between 30 degree and 60 degree injection was again negligible, but the 0 degree plate displayed a noticeable variation of f with the cushion to trunk pressure ratio. In the last series of plates the f values for 0 degree and 30 degree injection are again quite consistent with the results of configurations 21, 22, 23, 25 and 26. Injection at 60 degrees produced a noticeable variation in the value of f (similar to configuration 24).

The results show that Vaughan's theory can be used to predict the value of the flow coefficient if f is chosen in accordance with the above experimental results. Very generally, an f value of 0.85 applies to both the single and distributed peripheral jet configurations. Seven of the nine configurations can be reasonably correlated using $f = 0.85$, while two configurations (24 and 29) show a definite dependence of f on the cushion to trunk pressure ratio.

Power-Height Parameter

It should be recalled that a low value of C_{hd} is desirable (see eq 1).

Figure 11a shows the performance of the single slot configurations. The behavior of the single slots at 0 and 30 degrees was contrary to the behavior of the other seven configurations, which exhibited a continuous decrease in the experimental value of C_{hd} as R was increased (up to the highest R tested). The performance of the single slot at 0 degrees was generally erratic, and seemingly unaffected by the value of R . The data for the single slot with 30 degree injection indicates that the injection is beneficial only at low values of R for this configuration. At values of R above 0.30 the performance is severely degraded. Since the performance of these first two configurations was unusual, several graphs of the raw data from the tests of these plates were made in an attempt to determine the cause of the abnormal behavior. All the data curves were well behaved, however. The cause is apparently due to the small values of nozzle flow and daylight clearance which existed during the testing of these plates, especially at

the higher values of R . For example, the daylight clearance for these plates at $R = 0.50$ is on the order of 0.050 in. and the nozzle flow is on the order of 4.0 cfs. Since both measurements are small the experimental values of C_{hd} for these plates are subject to considerable variation. The performance of the single slot with 60 degree flow injection is superior to the other single slots throughout the entire range of R .

Figure 11b shows the performance of the three plates with 192 holes. The solid curves again illustrate the values of C_{hd} predicted by Vaughan's theory for an f value of 0.85 and flow injection angles of 0, 30 and 60 degrees. For this series of plates the beneficial effect of both 30 degree and 60 degree flow injection as compared to zero degree injection is clearly shown. An injection angle of 60 degrees is superior throughout the entire range of R .

Figure 11c shows the performance of the three plates with four slots. The favorable effect of inward flow injection is again evident. In this case, however, the effects of 30 degree and 60 degree injection are almost identical at low values of R . Above R values of 0.40 the performance of the 60 degree flow injection is slightly better than the 30 degree flow injection.

Generally then, in each group of similar plates the benefit of inward flow injection on power-height performance was shown.

The first objective of this study was to determine the usefulness of Vaughan's theoretical expressions for C_Q and C_{hd} . It has been shown that the simplified constant thickness jet theory can predict the value of the flow coefficient C_Q if a value of f is chosen with due regard for

the injection angle and the cushion to trunk pressure ratio. The experimental results for the power-height parameter, however, show that the theory does not adequately predict the proper value of C_{hd} . The simplified theory always predicts better performance than is achieved experimentally. The predicted values of C_{hd} get closer to the experimental values as the cushion to trunk pressure ratio R increases (See Table VI). For the configurations tested the predicted values of C_{hd} ranged from only 23 to 71 percent of the experimental values between $R = 0.40$ and $R = 0.70$. Generally, the predicted C_{hd} value was 40 percent to 50 percent of the experimental value between $R = 0.40$ and $R = 0.70$. The discrepancy between the experimental and theoretical values of C_{hd} that appears in this study was also experienced by Digges for two other inviscid momentum theories. Vaughan reports that the experimental C_{hd} results of this study correlate well with the data from tests conducted by Han.

The second objective of this study was to determine which of the nine nozzle configurations tested resulted in the lowest experimental value of C_{hd} . The single 60 degree slot demonstrated the best performance for R values less than or equal to 0.50. For values of R greater than 0.50 the performance of the 192 holes at 60 degrees and the four slots at 60 degrees was almost identical to each other. The performance of the four slots was just slightly better than that of the 192 holes between R values of 0.50 to 0.70.

R Config	.25	.30	.35	.40	.45	.50	.55	.60	.65	.70	.75	.80	.85	.90
0° Slot	.648	.778	.779	.861	.835	.871	.858	.897	.900	a				
30° Slot	.866	1.00	.940	.958	.926	.929	.929							
60° Slot	.694	.924	.859	.951	.887	.928	.868	.870	.848	.872				
0° Holes	.414	.436	.481	.505	.533	.552	.605	.615	.645	.652	.707	.717	.755	.785
30° Holes	.875	.867	.842	.844	.839	.827	.835	.838	.832	.835	.840	.847	.852	.865
60° Holes	.822	.826	.843	.832	.825	.832	.831	.830	.823	.839	.833	.850	.862	.869
0° Slots	.764	.776	.763	.786	.790	.800	.814	.821	.835	.839	b	.870	.884	.988
30° Slots	.659	.667	.699	.712	.731	.761	.778	.800	.809	.834	.848	.865	.873	.890
60° Slots	.282	.327	.331	.390	.393	.450	.500	.555	.611	.668	.693	.744	.816	.842

a Blank space indicates that the value of $R (P_c / P_t)$ could not be obtained.

b Bad data point.

Table II. f Values for Use in the Simplified Theory to Duplicate Experimental Flow Coefficient Results

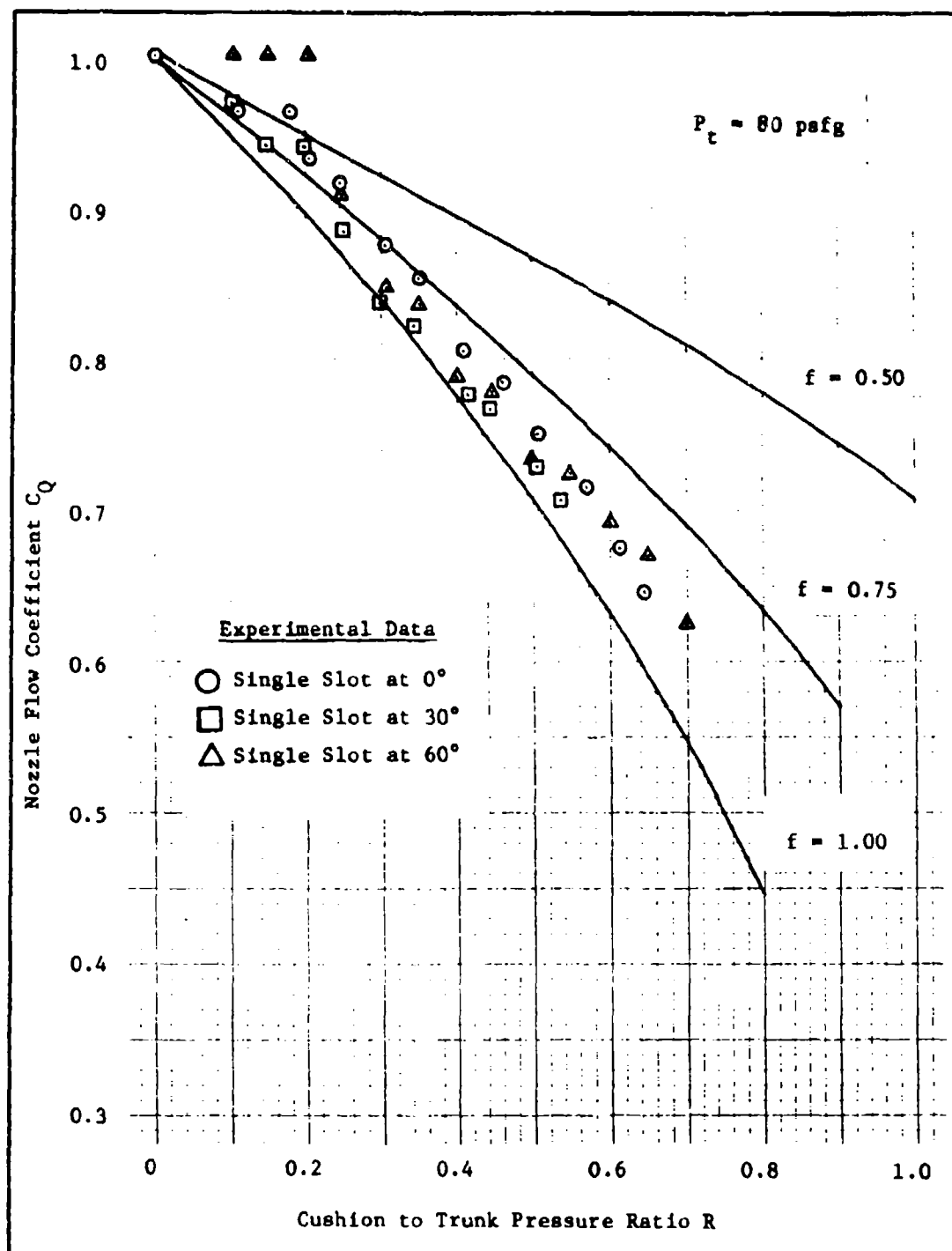


Fig. 10a. Effect of Varying Pressure Ratio on Flow Coefficient, Single Slot Configurations

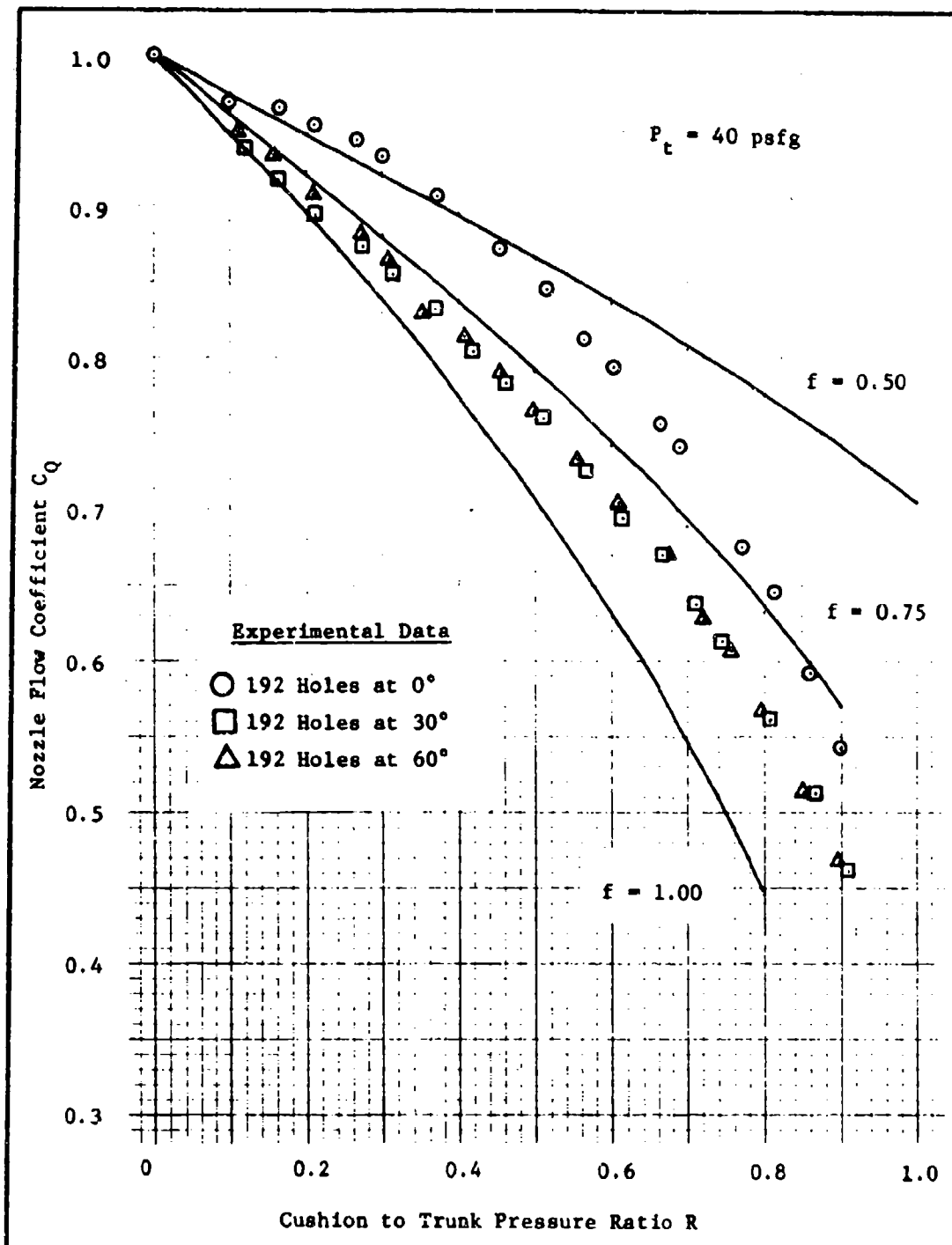


Fig. 10b. Effect of Varying Pressure Ratio on Flow Coefficient, 192 Hole Configurations

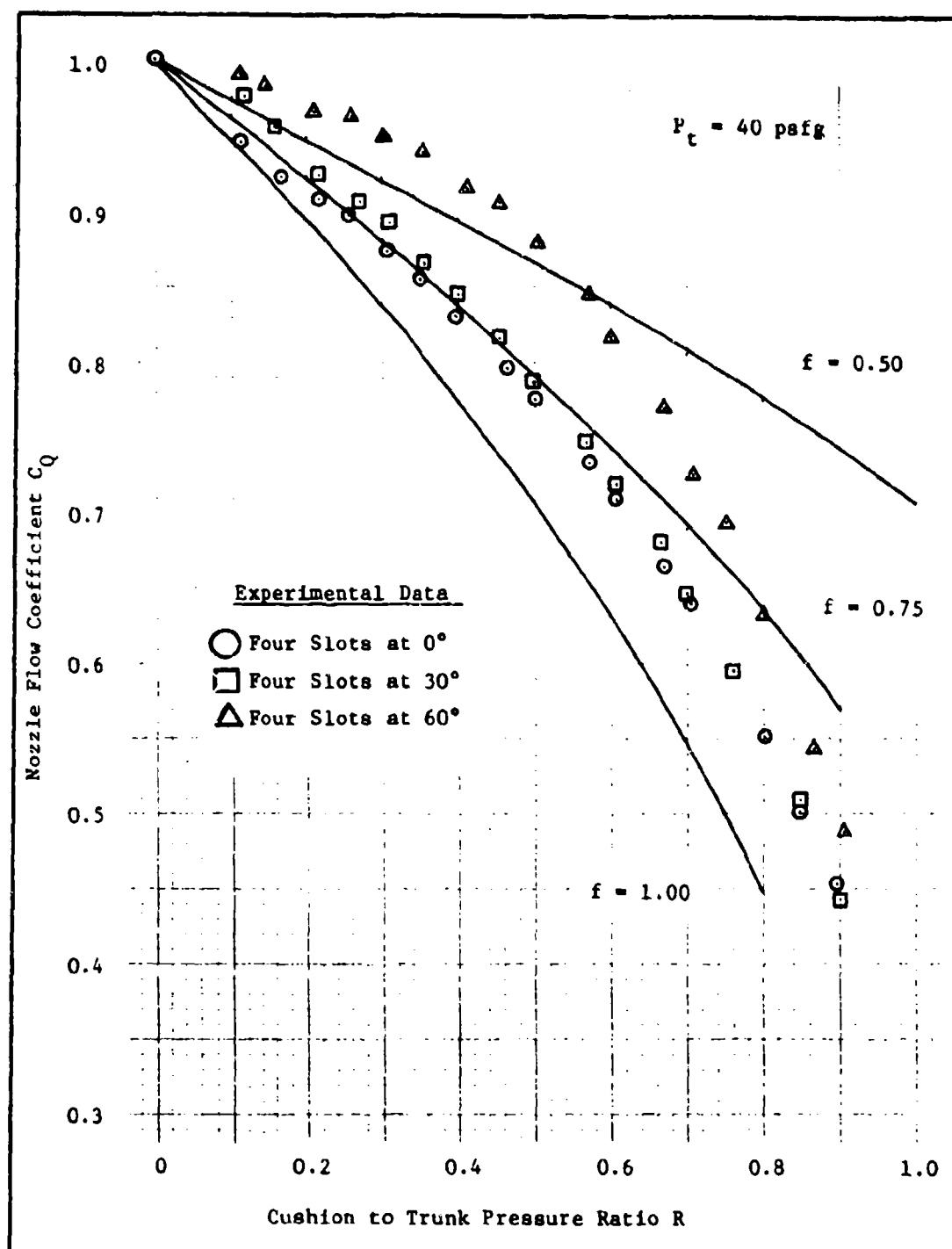


Fig. 10c. Effect of Varying Pressure Ratio on Flow Coefficient, Four Slot Configurations

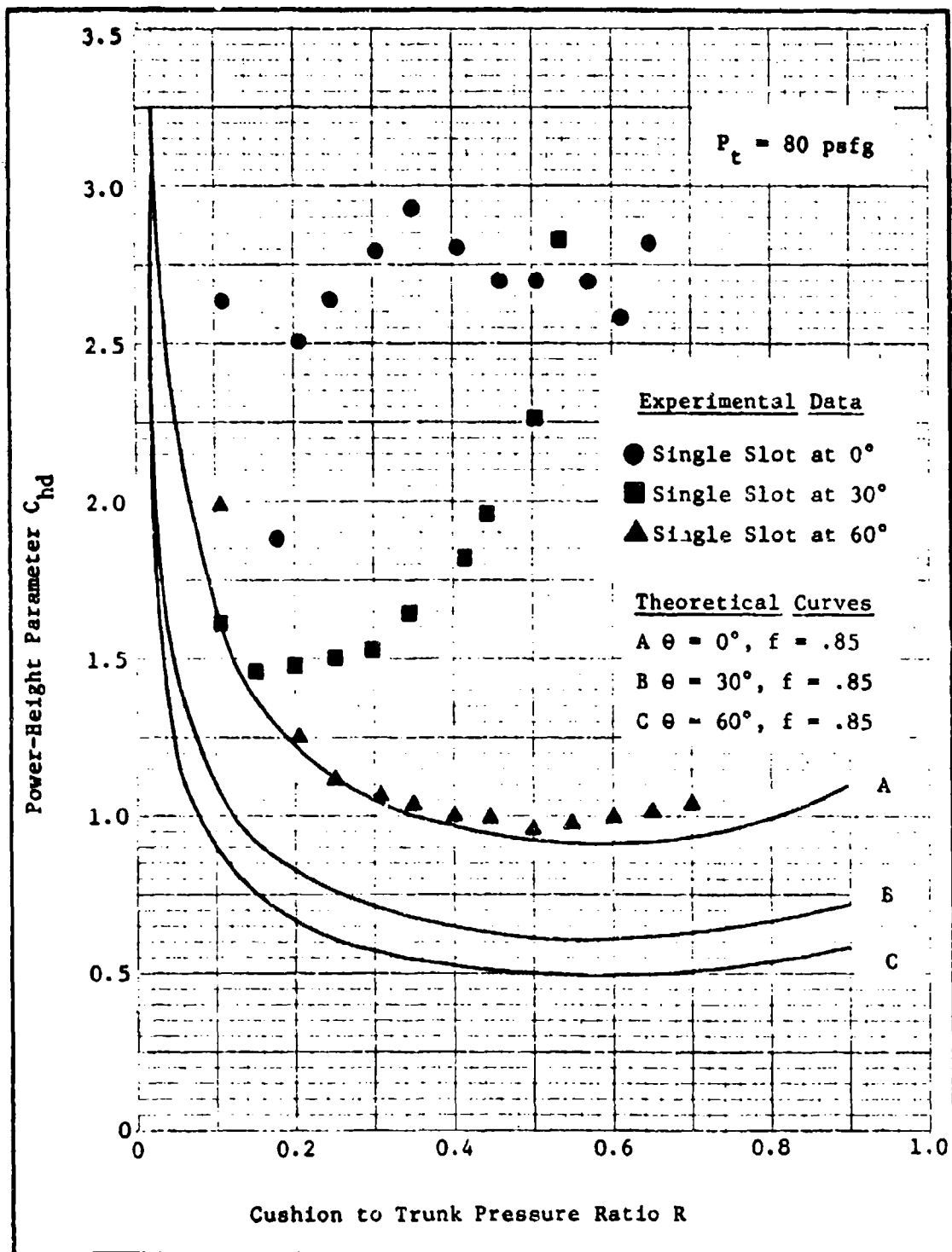


Fig. 11a. Variation of Power-Height Parameter with Cushion to Trunk Pressure Ratio, Single Slot Configurations

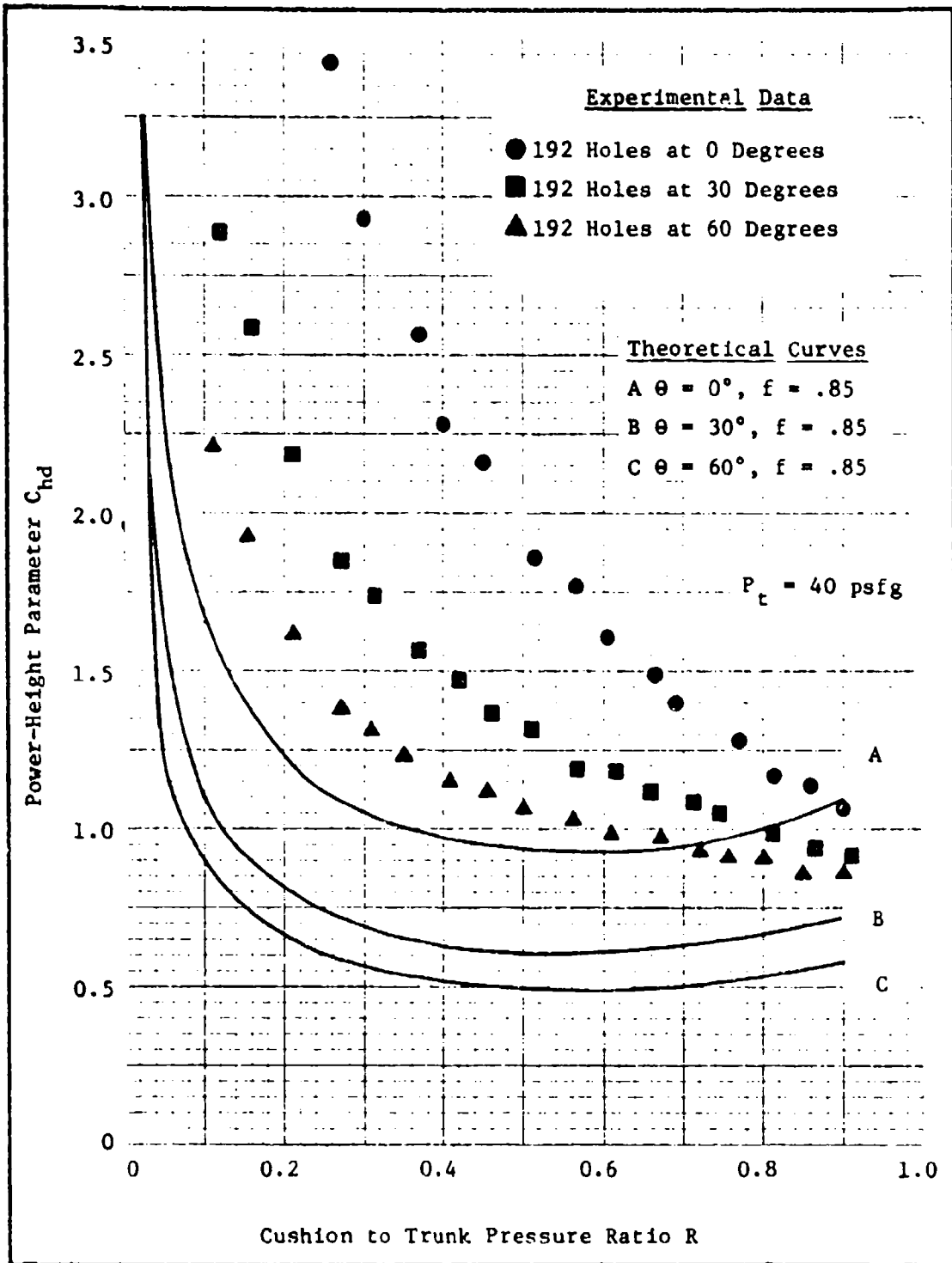


Fig. 11b. Variation of Power-Height Parameter with Cushion to Trunk Pressure Ratio, 192 Hole Configurations

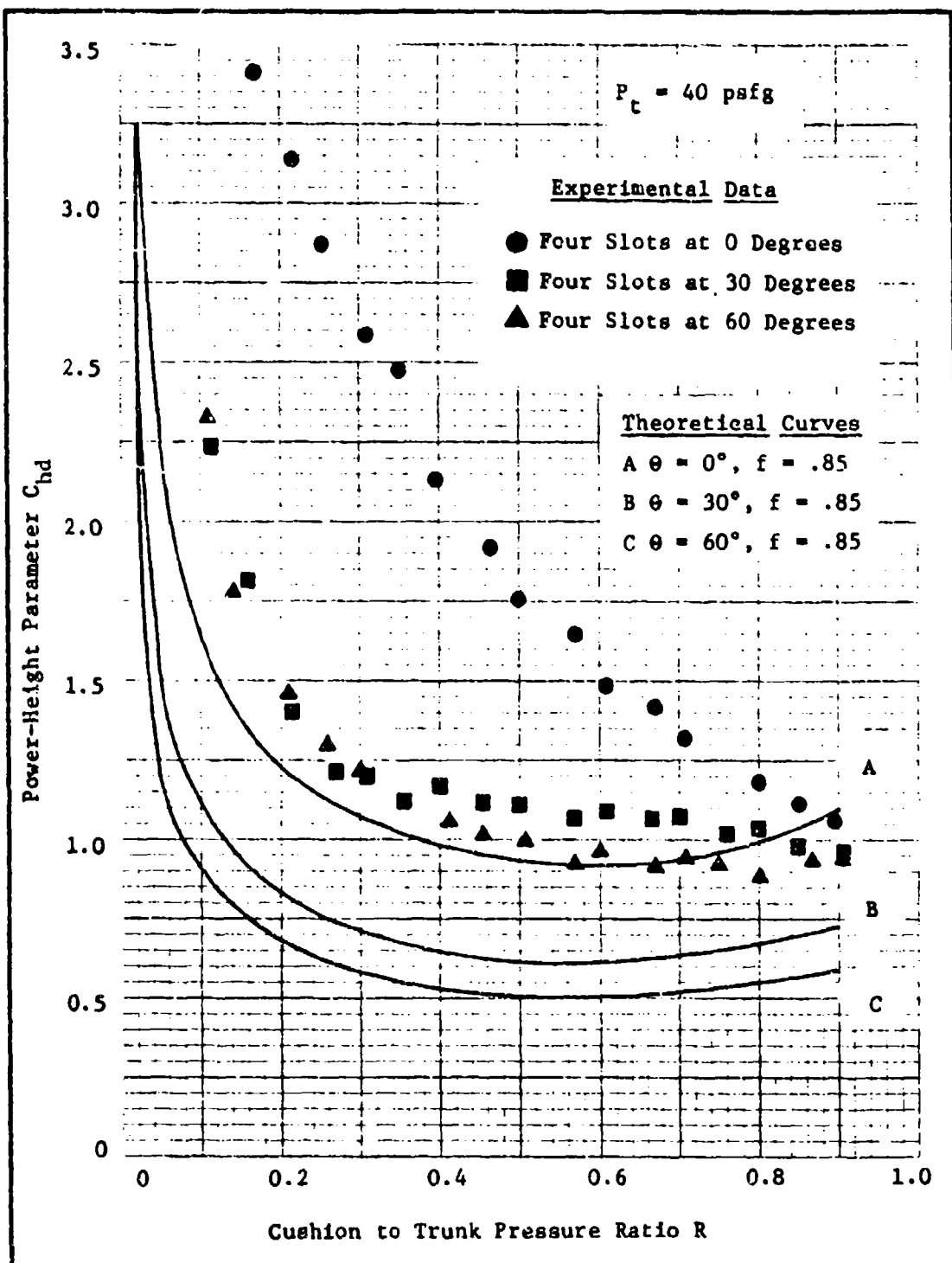


Fig. 11c. Variation of Power-Height Parameter with Cushion to Trunk Pressure Ratio, Four Slot Configurations

VI. Conclusions and Recommendations

Conclusions

Based on the results of this study the following conclusions are drawn:

(1) The concept of the f factor introduced in the simplified constant thickness jet theory can be used to predict experimental values of the flow coefficient C_Q which agree with experimental results.

(2) Theoretical values of C_{hd} predicted by the simplified constant thickness jet theory always indicate better performance than is achieved experimentally. Thus it appears that an efficiency factor must be applied to the theoretical (predicted) values of C_{hd} . The efficiency factor would range from 0.40 to 0.50 for cushion to trunk pressure ratios between 0.40 and 0.70.

(3) Although the predicted and experimental C_{hd} values for the distributed jet configurations did not agree quantitatively, the experimental data did behave qualitatively as the theory predicts.

(4) The beneficial effect of inward flow injection on power-height performance was demonstrated for all three groups of similar nozzle configurations. In the range of interest of R values, 60 degree flow injection resulted in roughly a 60 percent performance improvement over 0 degree injection.

(5) The values of the f factor and the experimental power-height parameter C_{hd} were extremely sensitive to small changes in the leakage flow rate and the daylight clearance, respectively.

Recommendations

(1) A solid test section should be used for further two-dimensional tests. Every effort must be made to eliminate leakage downstream of the flow measuring orifice.

(2) A more rigid floor and test section should be used to eliminate variations in daylight clearance across the width of the test section. A more convenient means of varying the floor height and measuring daylight clearance is desirable.

(3) A two-dimensional section of the actual trunk used on the CC-115 ACLS should be tested to see if any correlation exists between two-dimensional and three-dimensional power-height performance data.

(4) A flow visualization study of the trunk and nozzle region should be conducted to investigate possible Coanda and/or entrainment effects.

Bibliography

1. Air Force Flight Dynamics Laboratory. Static and Drop Tests of Quarter Scale Model of the CC-115 Aircraft Equipped with an Air Cushion Landing System. Technical Memorandum AFFDL-TM-72-01-FEM. Wright-Patterson Air Force Base, Ohio: AFFDL, January 1972.
2. American Society of Mechanical Engineers. Fluid Meters, Their Theory and Application (Sixth Edition). New York: ASME, 1971.
3. Digges, Kennerly H. Theory of an Air Cushion Landing System for Aircraft. Technical Report AFFDL-TR-71-50. Wright-Patterson Air Force Base, Ohio: Air Force Flight Dynamics Laboratory, June 1971.
4. Gorman, Dennis M. Equilibrium Characteristics of a Distributed Peripheral Jet. Unpublished thesis. Wright-Patterson Air Force Base, Ohio: Air Force Institute of Technology, March 1970.
5. Han, Lit S. Air Cushion Pressure During Stiff-Operation for Air Cushion Landing Systems. Technical Report AFFDL-TR-71-4, Part II. Wright-Patterson Air Force Base, Ohio: Air Force Flight Dynamics Laboratory, March 1972.
6. Vaughan, John C. A Simplified Peripheral Jet Theory to Describe Equilibrium Hover Performance of an Air Cushion Vehicle. Unpublished paper. Wright-Patterson Air Force Base, Ohio: Air Force Flight Dynamics Laboratory, February 1971.

Appendix A

A Simplified Peripheral Jet Theory to Describe Equilibrium

Hover Performance of an Air Cushion Vehicle

Introduction

A simplified model for this theory is shown in Fig. 12. The total airflow of the single peripheral jet is assumed to be the same as the total airflow of any given distributed jet. The injection angle of the flow is assumed to be such that the total momentum of the single peripheral jet is equal to the total momentum of the distributed jets. Finally, a control volume is placed around the area where the jet turns from its initial injection angle to become parallel to the ground.

Derivation of Theory

Assumptions for the Control Volume (Fig. 12)

- (1) Steady flow
- (2) Incompressible flow
- (3) The nozzle flow entering the control volume is subsonic (unchoked). Therefore the nozzle exit pressure of the jet is equal to the effective back pressure P_n .
- (4) Horsepower of air,

$$HP_{air} = \frac{(144)(P_t - P_a)(Q_n)}{550}$$

- (5) The jet enters the control volume at a speed equal to V_n and leaves the control volume parallel to the ground at a speed equal to kV_n , where k is a fraction. For purposes of this theory, it will be assumed that $k = 1.0$. Therefore, since the flow is steady and incompressible, this is the same as assuming that the jet turns at a constant flow thickness t and a constant velocity V_n .
- (6) The jet leaves the control volume at a static pressure equal to the ambient pressure P_a . Therefore, the flow is not isentropic, since the total pressure of the jet flow entering the control volume is greater than the total pressure of the flow leaving the control volume.

Definitions of Dimensionless Parameters

$$(1) \quad f = (P_n - P_a) / (P_c - P_a) \quad (2)$$

$$(2) \quad R = (P_c - P_a) / (P_t - P_a)$$

$$(3) \quad C_Q = V_n / V_a = \left[(P_t - P_n) / (P_t - P_a) \right]^{1/2}$$

$$(4) \quad C_{hd} = \frac{(HP_{air})(550)}{(144)(d)(S)(2g_c/\rho)^{1/2}(P_c - P_a)^{3/2}}$$

Governing Equations

(1) Continuity (for the nozzle)

$$Q_n = m / \rho = \frac{StV_n}{12} = \text{constant}$$

(2) Energy (for the nozzle for isentropic flow)

$$P_t = P_n + \frac{\rho}{2g_c} \frac{(V_n)^2}{144}$$

(3) x-momentum (for the control volume)

$$(12)(P_c - P_a) S d = \frac{\rho}{g_c} Q_n V_n (k + \sin \theta)$$

Derivation of Expression for C_Q

Starting with the definition of C_Q , rearrange to put in terms

f and R :

$$\begin{aligned} C_Q &= \left[\frac{P_t - P_n}{P_t - P_a} \right]^{1/2} \\ &= \left[\frac{(P_t - P_a) - (P_n - P_a)}{(P_t - P_a)} \right]^{1/2} \\ &= \left[1 - \frac{(P_n - P_a)(P_c - P_a)}{(P_t - P_a)(P_c - P_a)} \right]^{1/2} \end{aligned}$$

$$C_Q = (1 - fR)^{1/2} \quad (3)$$

Derivation of Expression for t/d

The x-momentum equation is

$$(12)(P_c - P_a) Sd = \frac{\rho}{g_c} Q_n V_n (k + \sin \theta)$$

use the continuity equation to eliminate Q_n

$$(12)(P_c - P_a) Sd = \frac{\rho}{g_c} \frac{St V_n^2}{12} (k + \sin \theta)$$

use the energy equation to eliminate V_n^2

$$V_n^2 = (P_t - P_n) 2g_c 144 / \rho$$

$$(P_c - P_a) Sd = 2(k + \sin \theta) St (P_t - P_n)$$

Rearrange to form t/d

$$t/d = \left[\frac{(P_c - P_a)}{2(k + \sin \theta)(P_t - P_n)} \right] \left[\frac{(P_t - P_a)}{(P_t - P_a)} \right]$$

$$t/d = \frac{R}{2(k + \sin \theta) C_Q^2}$$

Derivation of Expression for C_{hd}

$$C_{hd} = \left(\frac{HP_{air}}{144d} \right) \left(\frac{550}{S} \right) \left[\frac{1}{(2g_c / \rho)^{1/2}} \right] \left[\frac{1}{(P_c - P_a)^{3/2}} \right]$$

substituting for HP_{air} and Q_n ,

$$C_{hd} = \frac{(P_t - P_a)(S)(t)(V_n)}{(12)(S)(d)(P_c - P_a)^{3/2}(2g_c / \rho)^{1/2}}$$

Rearrange and eliminate V_n ,

$$C_{hd} = \left(\frac{t}{d} \right) \left(\frac{P_t - P_a}{P_c - P_a} \right) \left[\frac{(P_t - P_a)^{1/2}(2g_c / \rho)^{1/2}}{(P_c - P_a)^{1/2}(2g_c / \rho)^{1/2}} \right] \left[\frac{(P_t - P_a)^{1/2}}{(P_t - P_a)^{1/2}} \right]$$

$$C_{hd} = \frac{t}{d} \frac{C_Q}{R^{3/2}}$$

substituting for t/d ,

$$C_{hd} = \frac{1}{2(k + \sin \theta) C_Q R^{1/2}} \quad (4)$$

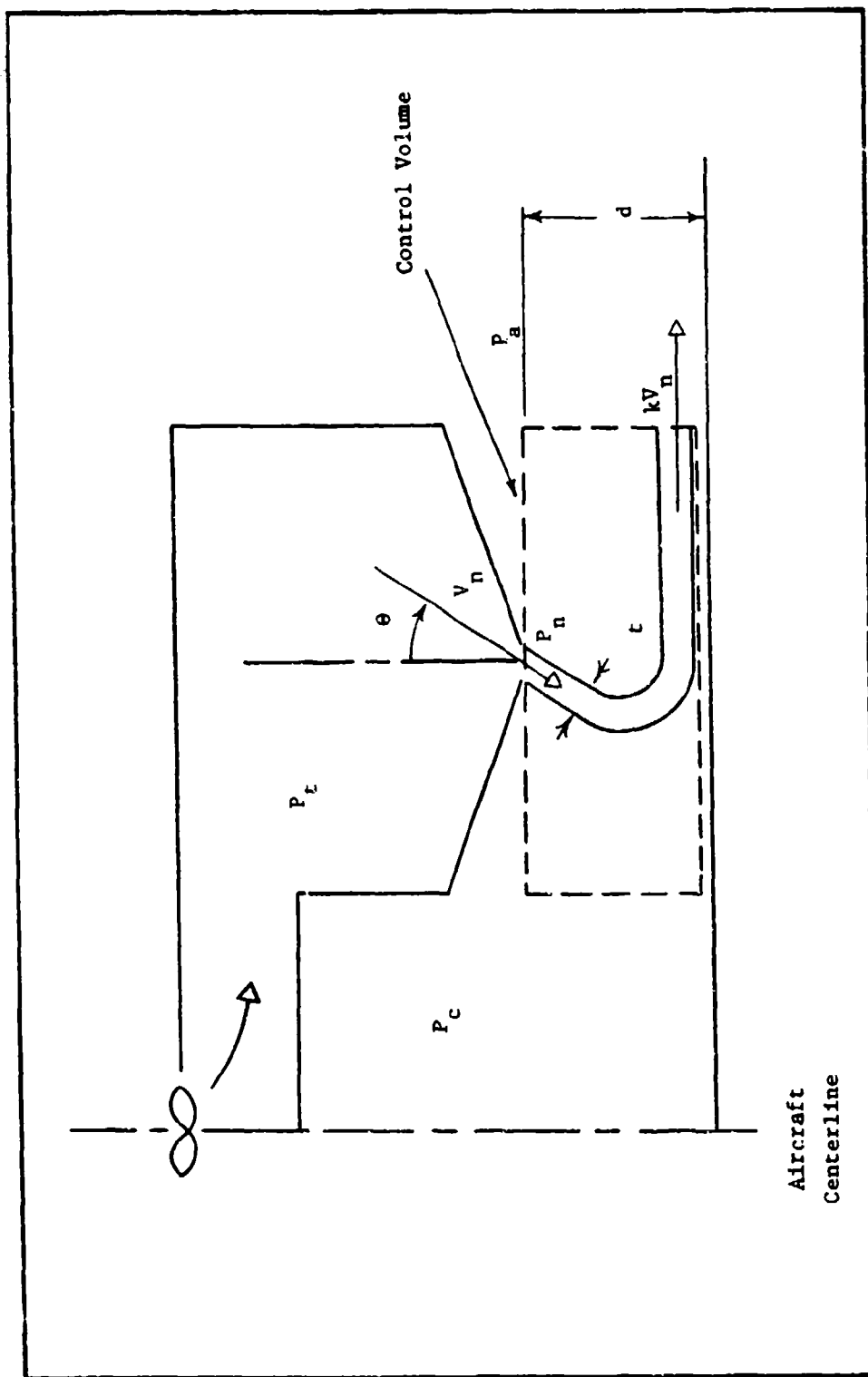


Fig. 12. Model for Simplified Peripheral Jet Theory

Appendix B

Derivation of Flow Rate Equations from the ASME Fluid Meters Report

Two square-edged orifice plates were constructed and used for the measurement of the flow rate of air to the test section. The ASME Fluid Meters Report (6th ed., 1971) develops the general expressions for the calculation of flow rate using various types of metering devices. The report also contains tables of empirical factors to be used when tailoring the general flow rate expressions to a particular type and size device and operating conditions. The following describes the derivation of the specific flow rate equations for the 2.4 in. diameter and 3.6 in. diameter square-edged orifices with flange pressure taps used in this study. All references are to the Fluid Meters Report.

The general flow rate expression for a differential pressure meter is:

$$m = 0.52502 \left[\frac{C}{(1-\beta^4)^{1/2}} \right] Y_1 d^2 F_a \left[\rho_1 (P_1 - P_2) \right]^{1/2} \quad (5)$$

where m is the flow rate in lbm/sec

C is the orifice coefficient of discharge

β is the ratio of the orifice diameter to the duct diameter

Y_1 is a net expansion factor

d is the orifice diameter in in.

F_a is a thermal expansion factor

ρ_1 is the density in lbm/ft^3 computed with the perfect gas law
using the upstream pressure and temperature

P_1 is the upstream orifice pressure in psia

P_2 is the downstream orifice pressure in psia

This general expression will now be developed to apply specifically to the 3.6 in. diameter orifice. The derivation for the 2.4 in. diameter orifice proceeds identically.

Given: $d = 3.6$ in. $D = 12.0$ in. $\beta = \frac{d}{D} = .30$

from Table II-I-1, $\frac{1}{(1 - \beta^4)^{1/2}} = 1.00407$

from Figure II-1-3, $F_a = 1.0$ for the range of temperatures encountered during testing

The general flow rate equation may now be rewritten as

$$m = 0.52716 C Y_1 d^2 \left[\rho_1 (P_1 - P_2) \right]^{1/2}$$

Values of C are given in Tables II-III-2 for duct diameters of certain sizes. Since there is no Table for the 12.0 in. duct used in this study the value of C may be computed with the general equations which were used to generate the data for Table II-III-2. This method of

obtaining a value for C is given in section I-5-38. Values of C were thus calculated for the 2.4 in. and 3.6 in. orifices for Reynolds numbers (based on the orifice diameter d) from 100,000 to 500,000 in increments of 100,000. Based on the flow rates from previous tests this was estimated to be the range of Reynolds numbers to be encountered during this study. For the 2.4 in. orifice the value of C varied from 0.6032 at $Re_d = 100,000$ to 0.5996 at $Re_d = 500,000$. Since the values were so close the C value of 0.6002 at $Re_d = 300,000$ was used for the remainder of the development. Likewise for the 3.6 in. orifice the C value of 0.6007 at $Re_d = 300,000$ was used. Thus the flow rate equation for the 3.6 in. diameter orifice may be written as

$$m = (0.52716) (0.6007) (3.6)^2 Y_1 \left[\rho_1 (P_1 - P_2) \right]^{1/2}$$

or

$$m = 4.104 Y_1 \left[\rho_1 (P_1 - P_2) \right]^{1/2}$$

Y_1 is given by

$$Y_1 = 1 - (0.41 + 0.35\beta^4) \left[\frac{(P_1 - P_2)}{(1.4 P_1)} \right]$$

where P_1 and P_2 are the absolute pressures upstream and downstream of the orifice, respectively. For the 3.6 in. orifice ($\beta = 0.3$) this becomes

$$Y_1 = 0.7051 + 0.2949 \left(\frac{P_2}{P_1} \right)$$

So the final expression for the mass flow rate for the 3.6 in. diameter orifice becomes

$$m = \left[2.8937 + 1.2102 \left(\frac{P_2}{P_1} \right) \right] \left[\rho_1 (P_1 - P_2) \right]^{1/2}$$

The same procedure was performed for the 2.4 in. diameter orifice and the final mass flow rate expression becomes

$$m = \left[1.2842 + 0.5322 \left(\frac{P_2}{P_1} \right) \right] \left[\rho_1 (P_1 - P_2) \right]^{1/2}$$

Figure 13 depicts the nozzle flow rate which existed for each nozzle configuration throughout a range of trunk pressures.

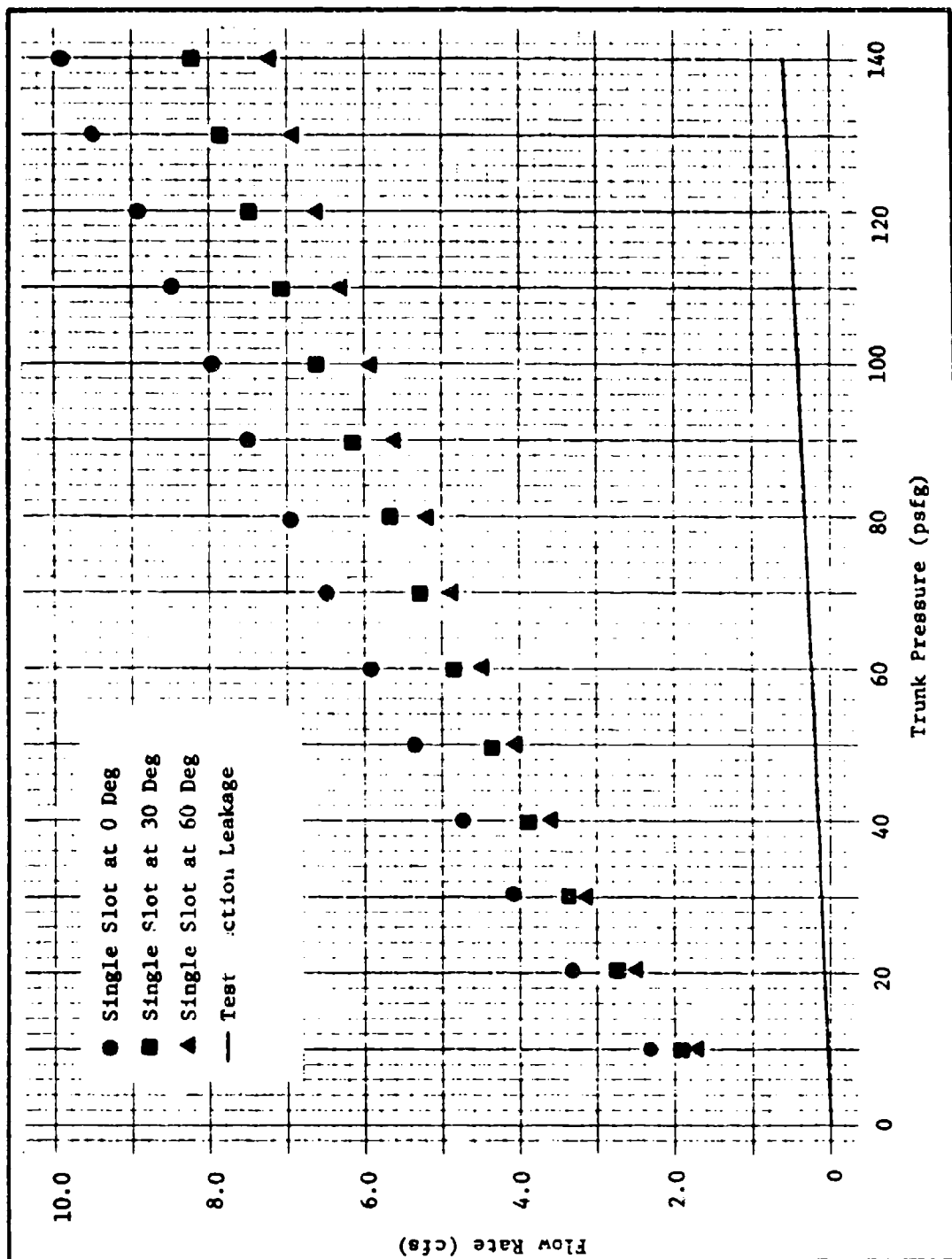


Fig. 13a. Total Flow Rate Variation with Trunk Pressure, Single Slot Configurations

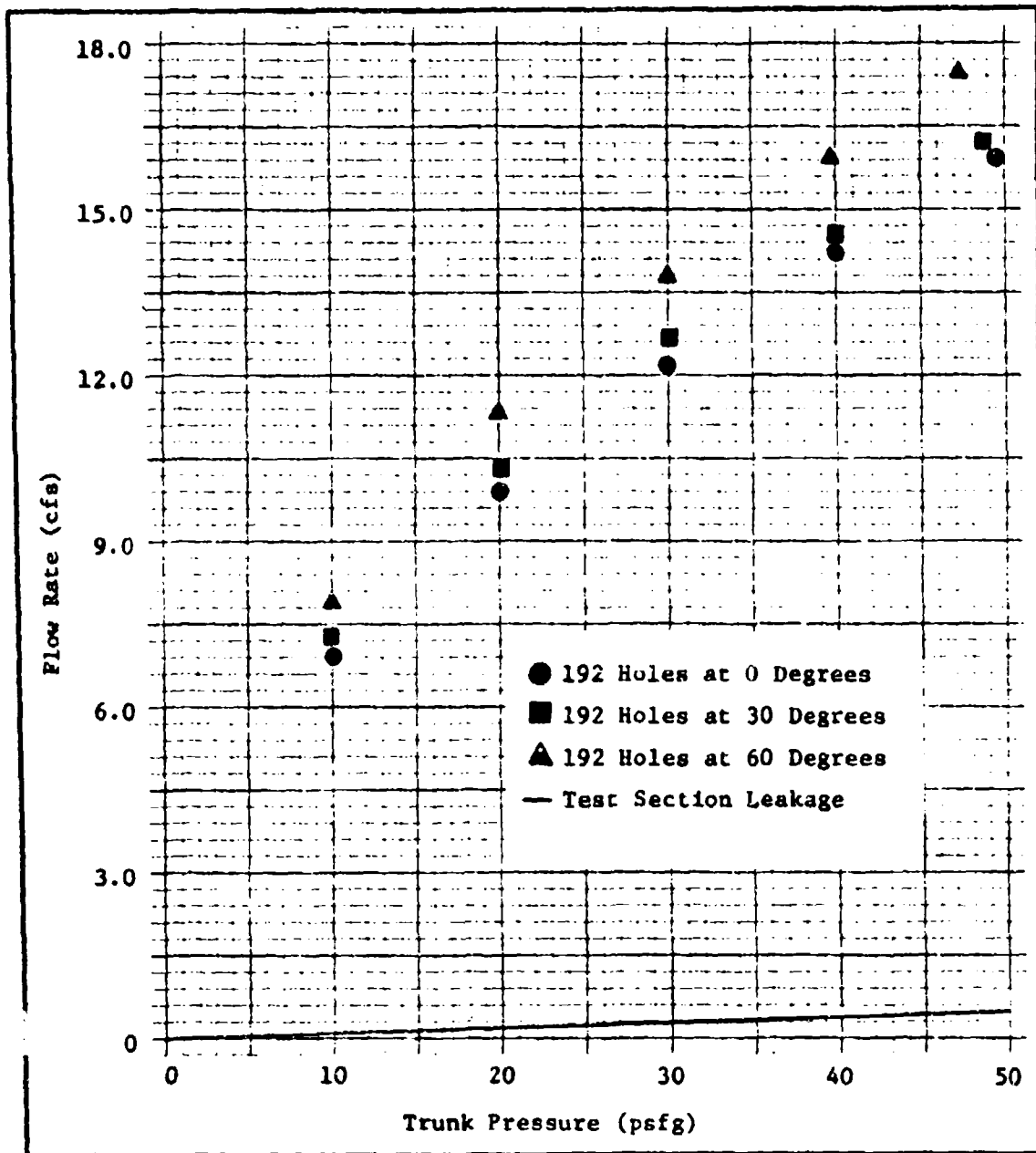


Fig. 13b. Total Flow Rate Variation with Trunk Pressure, 192 Hole Configurations

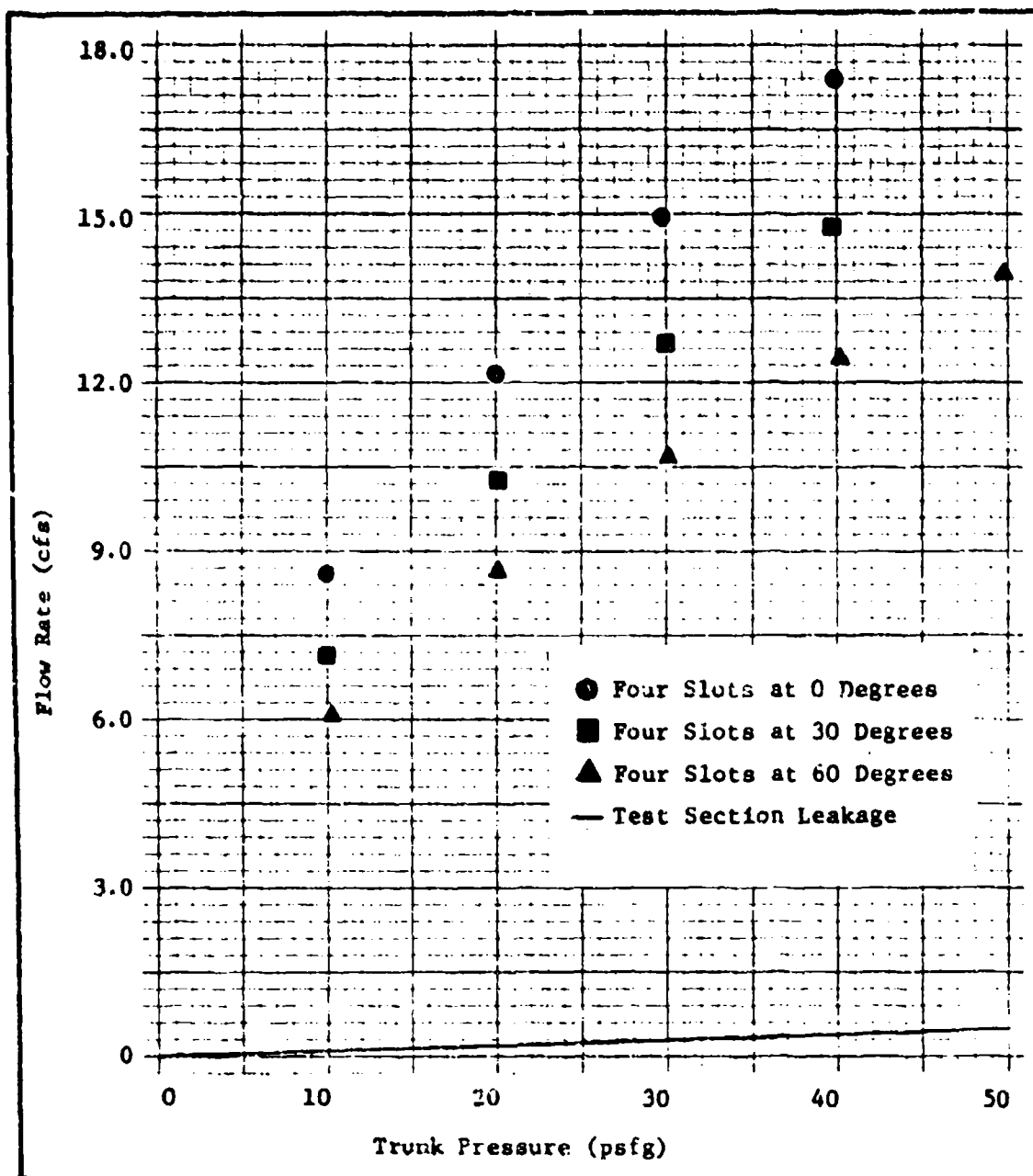


Fig. 13c. Total Flow Rate Variation with Trunk Pressure, Four Slot Configurations

Appendix C

Calculation of Test Section Leakage

The 2.4 in. diameter square-edged orifice was installed for all leakage tests. The following data was recorded during each test:

- P_a (ambient pressure in in. Hg)
- T_a (ambient temperature in C)
- T_{orif} (orifice temperature in C)
- P_{up} (upstream orifice pressure in in. H₂O)
- P_{down} (downstream orifice pressure in in. H₂O)
- P_t (trunk pressure in in. H₂O)

The following expression, developed in Appendix B, was used to compute the flow rate in lbm/sec:

$$\dot{m} = \left[1.2842 + 0.5322 \left(\frac{P_2}{P_1} \right) \right] \left[\rho_1 (P_1 - P_2) \right]^{1/2} \quad (7)$$

where P_1 is the upstream orifice pressure in psia

P_2 is the downstream orifice pressure in psia

ρ_1 is the density in lbm/ft³ computed with the perfect gas law using the upstream pressure and temperature

The entire mass flow rate thus measured represents test section leakage because a solid nozzle plate was installed for the test. To

convert this mass flow rate into a volumetric flow rate a density was computed using ambient pressure and the system (orifice) temperature.

A mass flow rate and a volumetric flow rate were thus computed for the entire range of trunk pressures used during the subsequent tests.

The Fortran program shown in Fig. 14 was used to calculate the leakage using the above procedure.

```

PROGRAM LEAK (INPUT, OUTPUT)
C THIS PROGRAM CALCULATES THE LEAKAGE FLOW RATE (QLEAK) FOR A GIVEN
C TRUNK FOR THE ENTIRE RANGE OF TRUNK PRESSURES USED IN TESTS.
C ENTER DATA IN THE FOLLOWING UNITS:
C   TESTNR (TEST NUMBER)
C   TRUNK (CODE NUMBER ASSIGNED TO EACH TRUNK)
C   PUP (UPSTREAM ORIFICE PRESSURE) IN INCHES OF WATER
C   PDOWN (DOWNSTREAM ORIFICE PRESSURE) IN INCHES OF WATER
C   PTGAGE (GAGE TRUNK PRESSURE) IN INCHES OF WATER
C   PAMB (AMBIENT PRESSURE) IN INCHES OF MERCURY
C   TC (ORIFICE TEMPERATURE) IN DEGREES CENTIGRADE
C   DORIF (ORIFICE DIAMETER) IN INCHES
C   ENDATA (A DUMMY VARIABLE TO INDICATE LAST DATA CARD)
C   INTEGER TESTNR, TRUNK, ENDATA
C   REAL QDOT
C
C   Z=1.0
10 READ 20, TESTNR, TRUNK, PUP, PDOWN, PTGAGE, PAMB, TC, DORIF, ENDATA
20 FORMAT (2I10, 6F8.4, I10)
C PCON CONVERTS PRESSURE FROM INCHES OF WATER TO PSI
PCON=.03613
PTGAGE=PTGAGE*PCON
PTPSF=PTGAGE*144.
P1=PUP*PCON+PAMB*.4912
P2=PDOWN*PCON+PAMB*.4912
PA=PAMB*.4912
C T1 IS THE ORIFICE TEMP CONVERTED TO RANKINE
T1=1.8*(TC+273.16)
RPG1=(144.*P1)/(53.3525*T1)

```

Fig. 14. Fortran Program for the Calculation of Test Section Leakage

```

C THE FOLLOWING FLOW RATE EQNS WERE DERIVED FROM THE ASME FLUID METERS
C REPORT (6TH ED, 1971) AND ARE BASED ON A DUCT DIAMETER OF 12 INCHES
C THE EXPRESSIONS APPLY ONLY TO SQUARE-EDGED ORIFICES OF DIAMETER
C INDICATED WITH FLANGE PRESSURE TAPS
C DORIF=2.4 FOR LEAK TESTS ; DORIF=3.6 FOR NOZZLE TESTS
C THE OTHER EQNS WERE PREVIOUSLY USED AND ARE LEFT FOR FUTURE REFERENCE
  IF(DORIF.EQ.1.2) MDOT=(0.3204+0.1327*(P2/P1))*SQRT(RH01*(P1-P2))
  IF(DORIF.EQ.2.4) MDOT=(1.2842+0.5322*(P2/P1))*SQRT(RH01*(P1-P2))
  IF(DORIF.EQ.3.0) MDOT=(2.005 +0.8343*(P2/P1))*SQRT(RH01*(P1-P2))
  IF(DORIF.EQ.3.6) MDOT=(2.8937+1.2102*(P2/P1))*SQRT(RH01*(P1-P2))
  IF(DORIF.EQ.5.0) MDOT=(5.612 +2.410 *(P2/P1))*SQRT(RH01*(P1-P2))
  IF(DORIF.EQ.6.0) MDOT=(8.156 +3.638 *(P2/P1))*SQRT(RH01*(P1-P2))
  RHOA=(144.*PA)/(53.3525*T1)
80 QLEAK=MDOT/RHOA
  IF(Z.GT.1.0) GO TO 50
30 PRINT 40
40 FORMAT (///T10*TEST NO. *,T25*TRUNK*,T40*PT (PSF)*,T58*ACTUAL LEAK
  1AGE (CFM)*,T95*ACTUAL LEAKAGE (LBM/SEC)* )
50 PRINT 60,TESTNR,TRUNK,PTPSF,QLEAK,MDOT
60 FORMAT (//I1X,I3,I1X,I2,I1X,F8.3,16X,F7.3,21X,F8.3)
  Z=Z+1.0
  IF(ENDATA.EQ.1) GC TO 70
  GO TO 10
70 CONTINUE
  END

```

Fig. 14 (cont'd). Fortran Program for the Calculation of Test Section Leakage

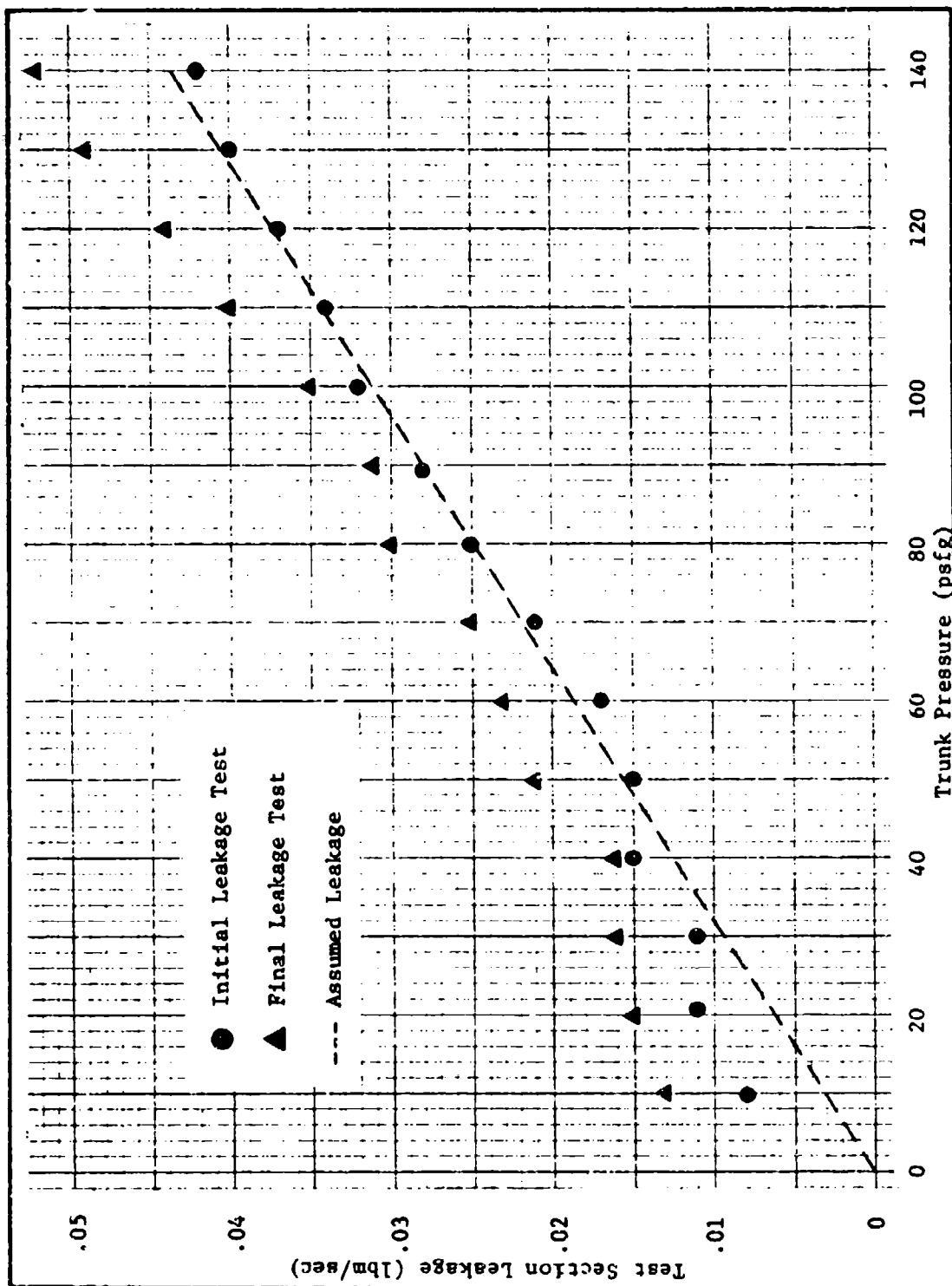


Fig. 15. Test Section Leakage Variation with Trunk Pressure

Appendix D

Calculation of Nozzle Discharge Coefficients

The 3.6 in. diameter square-edged orifice was installed for all coefficient of discharge tests. The following data was recorded during each test:

- P_a (ambient pressure in in. Hg)
- T_a (ambient temperature in C)
- T_{orif} (orifice temperature in C)
- P_{up} (upstream orifice pressure in in. H₂O)
- P_{down} (downstream orifice pressure in in. H₂O)
- P_t (trunk pressure in in. H₂O)

The following expression, developed in Appendix B, was used to compute the total flow rate in lbm/sec:

$$\dot{m} = \left[2.8937 + 1.2102 \left(\frac{P_2}{P_1} \right) \right] \left[\rho_1 (P_1 - P_2) \right]^{1/2}$$

where P_1 is the upstream orifice pressure in psia

P_2 is the downstream orifice pressure in psia

ρ_1 is the density in lbm/ft³ computed with the perfect gas law using the upstream pressure and temperature

The leakage mass flow rate for the existing trunk pressure was subtracted from the total mass flow rate to give the nozzle mass flow rate.

A density at the nozzle was computed with the perfect gas law using the ambient pressure and the system temperature. The nozzle mass flow rate was divided by the nozzle density to give the nozzle volumetric flow rate. An ideal ($C_D = 1$) volumetric flow rate for the nozzle was computed as:

$$Q_{\text{ideal}} \text{ (cfs)} = \frac{A_n}{144} \left[\frac{(144)(2g_c)(P_t - P_a)}{(\rho_t)} \right]^{1/2}$$

where A_n is the nozzle area in in.²

g_c is 32.2 ft-lbm/lbf-sec²

P_t is the trunk pressure in psia

P_a is the ambient pressure in psia

ρ_t is the nozzle density in lbm/ft³

The coefficient of discharge of the nozzle configuration is the ratio of the actual nozzle flow rate (at $P_c = P_a$) to the ideal nozzle flow rate:

$$C_D = \frac{Q_a}{Q_{\text{ideal}}}$$

A coefficient of discharge was thus determined for each nozzle configuration for a range of trunk pressures. The results are shown in Table III. The Fortran program shown in Fig. 16 was used to calculate the discharge coefficients using the above procedure.

P_t (psfg) Config.	10	20	30	40	50	60	70	80	90	100	110	120	130	140
21	.906	.902	.903	.906	.913	.918	.926	.931	.937	.945	.953	.962	.980	.987
22	.733	.731	.734	.726	.727	.731	.730	.733	.748	.760	.771	.782	.787	.793
23	.668	.670	.679	.672	.671	.673	.672	.668	.677	.679	.682	.685	.688	.686
24	.696	.701	.703	.707	.709	This data not taken due to limited airflow for large nozzle area configurations								
25	.720	.717	.719	.716	.721									
26	.790	.790	.790	.790	.793									
27	.880	.882	.883	.888	.891									
28	.742	.749	.754	.761	.763									
29	.643	.648	.652	.657	.659									

Table III. Nozzle Configuration Discharge Coefficients

```

PROGRAM CO (INPUT,OUTPUT)
C THIS PROGRAM CALCULATES THE NOZZLE DISCHARGE COEFFICIENT FOR EACH
C NOZZLE CONFIGURATION AND TRUNK PRESSURE COMBINATION OF THE 2-D FIG.
C ENTER DATA IN THE FOLLOWING UNITS0
C TESTNR (TEST NUMBER)
C TRUNK (A CODE NUMBER ASSIGNED TO EACH TRUNK)
C CONFIG (CODE NUMBER ASSIGNED TO EACH CONFIGURATION)
C PAMB (AMBIENT PRESSURE) IN INCHES OF MERCURY
C PTGAGE (GAGE TRUNK PRESSURE) IN INCHES OF WATER
C WLEAK (LEAKAGE IN LHM/SEC FROM PROGRAM LEAK)
C PUP (UPSTREAM ORIFICE PRESSURE) IN INCHES OF WATER
C PDOWN (DOWNSTREAM ORIFICE PRESSURE) IN INCHES OF WATER
C TC (ORIFICE TEMPERATURE) IN DEGREES CENTIGRADE
C DORIF (ORIFICE DIAMETER) IN INCHES
C AN (NOZZLE AREA) IN SQUARE INCHES
C ENDATA (DUMMY VARIABLE TO INDICATE LAST DATA CARD AND TO CONTROL
C PPINTOUT 9Y CONFIGURATION)
C INTEGER TESTNR,TRUNK,CONFIG,PAMB,PTGAGE,WLEAK,PUP,PDOWN,TC,DORIF,
C REAL MDOY
C Z=1.0
10 READ 20,TESTNR,TRUNK,CONFIG,PAMB,PTGAGE,WLEAK,PUP,PDOWN,TC,DORIF,
1AN,ENDATA
20 FORMAT(3I5,8F8.3,I1)
C PCON CONVERTS PRESSURE FROM INCHES OF WATER TO PSI
PCON=.03613
PTGAGE=PTGAGE*PCON
PTDSF=PTGAGE*144.
P1=PUP*PCON+PAMB*.4912
P2=PDOWN*PCON+PAMB*.4912
PA=PAMB*0.4912

```

Fig. 16. Fortran Program for the Calculation of Nozzle Discharge Coefficients

```

C T1 IS THE ORIFICE TEMP CONVERTED TO RANKINE
      T1=1.8*(TC+273.16)
      RH01=((144.*P1)/(53.3525*T1)
      RHGA=((144.*PA)/(53.3525*T1)
C THE FOLLOWING FLOW RATE EQNS WERE DERIVED FROM THE ASME FLUID METERS
C REPORT (6TH ED, 1971) AND ARE BASED ON A DUCT DIAMETER OF 12 INCHES
C THE EXPRESSIONS APPLY ONLY TO SQUARE-EDGED ORIFICES OF DIAMETER
C INDICATED WITH FLANGE PRESSURE TAPS
C DORIF=2.4 OR 3.0 FOR LEAK TESTS ; DORIF=3.6 FOR NOZZLE TESTS
C THE OTHER EQNS WERE PREVIOUSLY USED AND ARE LEFT FOR FUTURE REFERENCE
      IF(DORIF.EQ.1.2) MDOT=(0.3204+0.1327*(P2/P1))*SQRT(RH01*(P1-P2))
      IF(DORIF.EQ.2.4) MDOT=(1.2842+0.5322*(P2/P1))*SQRT(RH01*(P1-P2))
      IF(DORIF.EQ.3.0) MDOT=(2.005 +0.8343*(P2/P1))*SQRT(RH01*(P1-P2))
      IF(DORIF.EQ.3.6) MDOT=(2.8937+1.2102*(P2/P1))*SQRT(RH01*(P1-P2))
      IF(DORIF.EQ.5.0) MDOT=(5.612 +2.410 *(P2/P1))*SQRT(RH01*(P1-P2))
      IF(DORIF.EQ.6.0) MDOT=(8.156 +3.638 *(P2/P1))*SQRT(RH01*(P1-P2))
      WLEAK=.00312*PTPSF
C THE CONSTANT .00312 IS THE SLOPE OF THE (ASSUMED) LINEAR LEAKAGE (LRM/SEC)
C VS. TRUNK PRESSURE (PSF) CURVE FOR THE ALUMINUM TRUNK
      WNOZ=MDOT-WLEAK
      TN=T1
      FN=PA
      RHON=((144.*PN)/(53.3525*TN)
      QNOZLE=WNOZ/RHON
      QLEAK=WLEAK/RHON
      CTOTAL=MDOT/RHON
      QIDEAL=(AN/144.)*SQRT((64.4*144.*PTGAGE)/RHON)
      DCOEFF=QNOZLE/QIDEAL
      CDAN=AN*DCOEFF
      IF(Z.GT.1.0) GO TO 50

```

Fig. 16 (cont'd). Fortran Program for the Calculation of Nozzle Discharge Coefficients

```

30 PRINT 40
40 FORMAT (///15*TEST NO.*,119*TRUNK*,132*CONF IG*,145*PT (PSF)*,164*
10TOTAL*,181*QNOZLE*,199*QLEAK*,1118*CD*,1129*CDAN*)
50 IF(ENDATA.EQ.2)GC TC 400
PRINT 60,TESTNR,TRUNK,CONF IG,PTPSF,OTOTAL,QNOZLE,QLEAK,DCOEFF,CDAN
60 FORMAT (///5X,I4,11X,I1,11X,I3,10X,F7.3,9X,F7.3,11X,F7.3,11X,F6.3,1
11X,F6.3,7X,F6.3)
IF(ENDATA.NE.2)GO TO 80
400 PRINT 500
500 FORMAT (6M1,15*TEST NO.*,119*TRUNK*,132*CONF IG*,145*PT (PSF)*,
1164*QIOTAL*,181*QNOZLE*,199*QLEAK*,1118*CD*,1129*CDAN*)
200 PRINT 300,TESTNR,TRUNK,CONF IG,PTPSF,OTOTAL,QNOZLE,QLEAK,DCOEFF,CDAN
1N
300 FORMAT (///5X,I4,11X,I1,11X,I3,10X,F7.3,9X,F7.3,11X,F7.3,11X,F6.3,1
11X,F6.3,7X,F6.3)
80 Z=Z+1.0
IF(ENDATA.EQ.1) GC TO 70
GO TO 10
70 CONTINUE
END

```

Fig. 16 (cont'd). Fortran Program for the Calculation of Nozzle Discharge Coefficients

Appendix E

Calculation of Nozzle Performance Parameters

The 3.6 in. diameter square-edged orifice was installed for all nozzle performance tests. The following data was recorded during each test:

- P_a (ambient pressure in in. Hg)
- T_a (ambient temperature in C)
- T_{orif} (orifice temperature in C)
- P_{up} (upstream orifice pressure in in. H_2O)
- P_{down} (downstream orifice pressure in in. H_2O)
- P_t (trunk pressure in in. H_2O)
- P_c (cushion pressure in in. H_2O)
- d (daylight clearance in in.)

The nozzle mass flow rate was calculated as described in Appendix D. A reference flow rate for the nozzle was calculated based on the effective nozzle area (actual nozzle area multiplied by the coefficient of discharge). This reference flow rate Q_a was calculated by assuming that the nozzle exit pressure was equal to P_a .

$$Q_a \text{ (cfs)} = \frac{C_D A_n}{144} \left[\frac{(144)(2g_c)(P_t - P_a)}{(\rho)} \right]^{1/2}$$

where $C_D A_n$ is the effective nozzle area in in.²

P_t is the trunk pressure in psia

P_a is the ambient pressure in psia

ρ is the nozzle density in lbm/ft³ computed with the perfect gas law using the cushion pressure and system temperature

At any other value of nozzle exit pressure, the experimental flow coefficient C_Q is the ratio of the existing nozzle flow to the reference ($P_n = P_a$) nozzle flow. The value of f was computed by rewriting Vaughan's theoretical expression for C_Q as:

$$f = \frac{1}{R} \left(1 - C_{Q_{exp}}^2 \right) \quad (8)$$

A trunk volumetric flow rate was computed by dividing the nozzle mass flow rate by a density ρ_t , which was calculated with the perfect gas law using the absolute trunk pressure and the system temperature.

The horsepower required to sustain the trunk flow rate and trunk pressure was calculated from:

$$HP_{air} = \frac{(P_t - P_a)(Q_n)(144)}{550}$$

where P_t is the trunk pressure in psia

P_a is the ambient pressure in psia

Q_n is the trunk flow rate in cfs

The experimental value of the power-height parameter C_{hd} was computed using Digges' expression

$$C_{hd} = \frac{(HP_{air})(550)}{(S)(d)(144)(P_c - P_a)^{3/2} \left[\frac{(2g_c)}{(\rho)} \right]^{1/2}} \quad (1)$$

where HP_{air} is in horsepower

S is the two-dimensional test section width in ft.

d is the daylight clearance in in.

P_c is the cushion pressure in psia

P_a is the ambient pressure in psia

g_c is 32.2 ft-lbm/lbf-sec²

ρ is the nozzle density in lbm/ft³ computed with the perfect gas law using the trunk pressure and system temperature

The theoretical value of C_Q was computed using Vaughan's expression

$$C_{Q_{thy}} = \left(1 - fR \right)^{1/2} \quad (3)$$

This value was then used to compute the theoretical value of C_{hd} using Vaughan's expression

$$C_{hd} = \frac{1}{2(k + \sin \theta)(C_{Q_{thy}})(R)^{1/2}} \quad (4)$$

The Fortran program shown in Fig. 17 was used to calculate the nozzle performance parameters using the above procedure.

```

PROGRAM DATA (INPUT,OUTPUT)
C THIS PROGRAM CALCULATES THE EXPERIMENTAL POWER JET HEIGHT PARAMETER (CHD) AND
C THE EXPERIMENTAL F FACTOR. IT ALSO CALCULATES THE THEORETICAL CHD AND CQ USING
C THE SIMPLIFIED JET THEORY. THE LEAKAGE FLOW RATES (WLEAK) AND THE NOZZLE
C DISCHARGE COEFFICIENTS (CD) ARE CALCULATED IN OTHER PROGRAMS.
C ENTER DATA IN FOLLOWING UNITS
C
C TESTNR (TEST NUMBER)
C CONFIG (A CODE NUMBER ASSIGNED TO EACH NOZZLE CONFIGURATION)
C THETA (NOZZLE INJECTION ANGLE; + FOR INJECTION TOWARD CUSHION, -
C FOR INJECTION TOWARD AMBIENT)
C PUP (UPSTREAM ORIFICE PRESSURE) IN INCHES OF WATER
C FDOWN (DOWNSTREAM ORIFICE PRESSURE) IN INCHES OF WATER
C PAMB (AMBIENT PRESSURE) IN INCHES OF MERCURY
C PCGAGE (GAGE CUSHION PRESSURE) IN INCHES OF WATER
C PTGAGE (GAGE TRUNK PRESSURE) IN INCHES OF WATER
C TC (ORIFICE TEMPERATURE) IN DEGREES CENTIGRADE
C DORIF (ORIFICE DIAMETER) IN INCHES
C COAN (EFFECTIVE NOZZLE AREA) IN SQUARE INCHES
C WLEAK (LEAKAGE IN LBM/SEC FROM PROGRAM LEAK)
C DAYLT (CLEARANCE BETWEEN TRUNK AND FLOOR) IN INCHES
C ENDATA (DUMMY VARIABLE TO INDICATE LAST DATA CARD AND TO CONTROL
C PRINTOUT BY CONFIGURATION)
C INTEGER CONFIG,TESTNR,ENDATA
C REAL MDOT
C Z=1.
10 READ 20,TESTNR,CONFIG,THETA,PUP,PDOWN,PAMB,PCGAGE,PTGAGE,TC,DORIF,
1COAN,WLEAK,CAYLT,ENDATA
20 FORMAT (2I4,F6.2,5F7.3,2F5.2,2F7.3,F6.3,I1)
IF (TESTNR.GE.496.AND.TESTNR.LE.502)COAN=3.222
IF (TESTNR.GE.784.AND.TESTNR.LE.797)COAN=3.434

```

Fig. 17. Fortran Program for the Calculation of Nozzle Performance Parameters

```

IF(TESTNR.GE.488.AND.TESTNR.LE.495)COAN=3.334
IF(TESTNR.GE.503.AND.TESTNR.LE.512)COAN=3.334
IF(TESTNR.GE.814.AND.TESTNR.LE.825)COAN=2.750
IF(TESTNR.GE.840.AND.TESTNR.LE.854)COAN=2.504
IF(TESTNR.GE.579.AND.TESTNR.LE.697)COAN=10.400
IF(TESTNR.GE.631.AND.TESTNR.LE.649)COAN=10.551
IF(TESTNR.GE.655.AND.TESTNR.LE.673)COAN=11.632
IF(TESTNR.GE.704.AND.TESTNR.LE.722)COAN=12.692
IF(TESTNR.GE.727.AND.TESTNR.LE.745)COAN=10.782
IF(TESTNR.GE.751.AND.TESTNR.LE.769)COAN=9.070
IF(TESTNR.GE.875.AND.TESTNR.LE.885)COAN=2.860
IF(TESTNR.GE.496.AND.TESTNR.LE.502)COT=.1074
IF(TESTNR.GE.784.AND.TESTNR.LE.797)COT=.1164
IF(TESTNR.GE.488.AND.TESTNR.LE.495)COT=.1111
IF(TESTNR.GE.503.AND.TESTNR.LE.512)COT=.1111
IF(TESTNR.GE.814.AND.TESTNR.LE.825)COT=.0916
IF(TESTNR.GE.840.AND.TESTNR.LE.854)COT=.0835
IF(TESTNR.GE.675.AND.TESTNR.LE.697)COT=.3358
IF(TESTNR.GE.631.AND.TESTNR.LE.649)COT=.3402
IF(TESTNR.GE.555.AND.TESTNR.LE.673)COT=.3735
IF(TESTNR.GE.704.AND.TESTNR.LE.722)COT=.4050
IF(TESTNR.GE.727.AND.TESTNR.LE.745)COT=.3745
IF(TESTNR.GE.751.AND.TESTNR.LE.769)COT=.2947
IF(TESTNR.GE.875.AND.TESTNR.LE.885)COT=.0968
C PCON CONVERTS PRESSURE FROM INCHES OF WATER TO PSI
PCON=.03513
F1=PIP*PCON+FAMR*.4912
P2=PD0WN*PCON+PAMB*.4912
PT=PTGAGE*PCON+PAMB*.4912
PC=PCGAGE*PCON+PAMR*.4912

```

Fig. 17 (cont'd). Fortran Program for the Calculation of Nozzle Performance Parameters

```

      PA=PAM**0.4912
      C T1 IS THE ORIFICE TEMP CONVERTED TO RANKINE
      T1=1.8*(TC+273.16)
      RH01=((144.*P1)/(53.3525*T1)
      PH0A=((144.*PA)/(53.3525*T1)
      TN=T1
      PN=PC
      RHOT=((144.*PT)/(53.3525*T1)
      RHON=((144.*PN)/(53.3525*TN)
      C THE FOLLOWING FLOW RATE EQNS WERE DERIVED FROM THE ASME FLUID METERS
      C REPORT (6TH ED, 1971) AND ARE BASED ON A DUCT DIAMETER OF 12 INCHES
      C THE EXPRESSIONS APPLY ONLY TO SQUARE-EDGED ORIFICES OF DIAMETER
      C INDICATED WITH FLANGE PRESSURE TAPS
      C DORIF=2.4 OR 3.0 FOR LEAK TESTS; DORIF=3.6 FOR NOZZLE TESTS
      C THE OTHER EQNS WERE PREVIOUSLY USED AND ARE LEFT FOR FUTURE REFERENCE
      IF(DORIF.EQ.1.2)MDO1=(6.3204+0.1327*(P2/P1))*SQRT(RH01*(P1-P2))
      IF(DORIF.EQ.2.4)MDO1=(1.2842+0.5322*(P2/P1))*SQRT(RH01*(P1-P2))
      IF(DORIF.EQ.3.0)MDO1=(2.005 +0.8343*(P2/P1))*SQRT(RH01*(P1-P2))
      IF(DORIF.EQ.3.6)MDO1=(2.8937+1.2102*(P2/P1))*SQRT(RH01*(P1-P2))
      IF(DORIF.EQ.5.0)MDO1=(5.612 +2.410 *(P2/P1))*SQRT(RH01*(P1-P2))
      IF(DORIF.EQ.6.0)MDO1=(8.156 +3.638 *(P2/P1))*SQRT(RH01*(P1-P2))
      PTPSF=PTGAGE*PCON*144.
      WLEAK=.000312*PTPSF
      C THE CONSTANT .000312 IS THE SLOPE OF THE (ASSUMED) LINEAR LEAKAGE (LBM/SEC)

```

Fig. 17 (cont'd). Fortran Program for the Calculation of Nozzle Performance Parameters

```

C VS. TRUNK PRESSURE (PSF) CURVE FOR THE ALUMINUM TRUNK
WNO7=M*DOT-MLEAK
QTOT=MDOT/RHON
QLEAK=MLEAK/RHON
QNOZLE=WNO2/RHON
QTRUNK=WNO7/RHON
TOVERO=CCT/DAYLT
C CALCULATION OF COEXP
PTGAGE=PTGAGE*PCON
QIDEAL=(CDAN/144.)*SORT((64.*144.*PTGAGE)/RHON)
COEXP=QNCZLE/QIDEAL
C CALCULATION OF R
R=PCGAGE/(PTGAGE/PCON)
PCPSF=R*FTPSF
C CALCULATION OF F
IF(PCGAGE.EQ.0.) F=1
IF(PCGAGE.EQ.0.) GO TO 21
F=(1/R)*(1-(COEXP**2))
IF(F.LT.0.0) F=0.0
C CALCULATION OF CHDEX
21 H-PATR=(144.*PTGAGE*QTRUNK)/550.
S=2.50
IF(DAYLT.LE..001.AND.Z.EQ.1.0) GO TO 30
IF(DAYLT.LE..001.AND.Z.GT.1.0) GO TO 90

```

Fig. 17 (cont'd). Fortran Program for the Calculation of Nozzle Performance Parameters

```

IF(DAYLT.EQ.99.9)CHDEXP=0.
IF(DAYLT.EQ.99.9)GO TO 25
IF(PCGAGE.EQ.0.)CHDEXP=0.
IF(PCGAGE.EQ.0.)GO TO 25
CHDEXP=(HPAIR*550.)/(S*DAYLT*144.*(PCGAGE*PCON)**1.5*(64.4/RHON)**
1.5)
C CALCULATION OF COTHY AND CHDTHY
25 COTHY=(1-(F*R))**.5
  THETA=THETA/57.2958
  IF(PCGAGE.EQ.0.) CHDTHY=0.
  IF(PCGAGE.EQ.0.) GO TO 26
  CHDTHY=1/(2.*(1.+SIN(THETA)))*COTHY*SQRT(R)
26 IF(Z.GT.1.0)GO TO 50
30 PRINT 40
40 FORMAT (///T2*TEST*,T9*CONFIG*,T19*THETA*,T27*PT(PSFG)*,T30*PC/FT
  1*,T40*ONozLE*,T59*DAYLT*,T69*CO(I/D)*,T91*HPAIR*,T92*F*,T99*COFXP*
  2,T108*FC(PSFG)*,T119*CHDEXP*,T130*CHDTHY*)
  IF(DAYLT.LE.001.AND.Z.EQ.1.0) GO TO 90
50 IF(ENDATA.EQ.2)GO TO 400
  PRINT 60,TESTNR,CCNFIG,THETA,PTPSF,R,ONozLE,DAYLT,TOVERD,HFAIR,F,C
  10EXP,PCPSF,CHDEXP,CHDTHY
60 FORMAT (// 1X,I3,5X,I3,5X,F6.3,2X,F6.3,2X,F6.3,5X,F7.3,5X,F5.3,4X,F
  17.3,4X,F7.3,3X,F5.3,5X,F5.3,5X,F6.3,4X,F6.3,5X,F6.3)
C A TRUNCATED VALUE OF DAYLT ON THE OUTPUT MEANS THAT THE FLOOR WAS

```

Fig. 17 (cont'd). Fortran Program for the Calculation of Nozzle Performance Parameters

```

C NOT IN THE TEST SECTION FOR THAT TEST: A DAYLT VALUE OF 99.9 WAS
C ENTERED ON THE DATA CARD FOR THIS CONDITION
      IF(ENDATA.NE.2)GO TO 80
400 PRINT 500
500 FORMAT (1H1      ,T2*TEST*,T9*CCNFIG*,T19*THETA*,T27*PT(PSFG)*,T38*PC
1/OT*,T48*QNOZLE*,T59*DAYLT*,T69*CD(T/D)*,T81*HPAIR*,T92*F*,T99*COE
2XP*,T108*PC(PSFG)*,T119*CHDEXP*,T130*CHOTHY*)
200 PRINT 300,TESTNR,CONFIG,THETA,PTFSF,R,QNOZLE,DAYLT,TOVERD,HPAIR,F,
1CQEXP,PCPSF,CHDEXP,CHOTHY
300 FORMAT (///1X,I3,5X,I3,5X,F6.2,3X,F7.3,2X,F6.3,5X,F7.3,5X,F5.3,4X,
1F7.3,4X,F7.3,3X,F5.3,5X,F5.3,5X,F6.3,4X,F6.3,5X,F6.3)
      IF(DAYLT.GT. 1.0E-03) GO TO 80
90 PRINT 100,TESTNR
100 FORMAT (///3X,I3,T15*DAYLIGHT CLEARANCE IS LESS THAN .001 INCH: FUR
1THER CALCULATIONS WERE SUPPRESSED*)
80 Z=Z+1.0
      IF(ENDATA.EQ.1)GO TO 70
      GO TO 10
70 CONTINUE
      END

```

Fig. 17 (cont'd). Fortran Program for the Calculation of Nozzle Performance Parameters

Appendix F

Effective Flow Injection Angle Investigation

A study was made to determine what flow injection angle actually existed for 5/16 in. diameter holes drilled at angles of 30, 45 and 60 degrees in a 1/4 in. thick aluminum plate. Configurations 25 and 26 in the study had holes drilled for inward injection at 30 degrees and 60 degrees, respectively. Since the nozzle plates were limited to a thickness of 1/4 in. by machining considerations, it was desired to determine what flow angle actually resulted. A sample of 1/4 in. thick plate was drilled with three 5/16 in. diameter holes, one each at 30 degrees, 45 degrees and 60 degrees. The plate was bolted to a calming chamber and connected to a compressed air source. The air pressure was set to duplicate the mass flow rate through the holes which existed for pressure differentials of 40 psfg and 80 psfg in the two-dimensional test section. A ram pressure probe mounted on a traverse was used to find the core of the flow issuing from the hole being tested. When the core was located the actual angle of the flow was determined from the location of the traverse. Table V gives the results of the investigation.

Table IV. Effective Nozzle Injection Angles

Trunk Pressure (psfg) Drilled Angle (Degrees)	40	80	120
30	18	23	18
45	34	33	35
60	41	45	42

Appendix G

Effect of Outward Injection on Nozzle Flow Rate

One series of tests was performed to determine what the effect on the nozzle flow rate would be if the nozzle plate was installed for outward injection. The nozzle flow rate for the plate with four slots at 60 degrees was determined for both inward and outward injection with cushion pressure equal to ambient pressure. The results are given in Table V.

Table V. Increase in Nozzle Flow Rate with Outward Injection

Trunk Pressure (psfg)	Nozzle Flow Rate (cfs)		Percent Increase with Outward Injection
	Inward Injection	Outward Injection	
10	6.04	6.67	10
20	8.55	9.31	9
30	10.56	11.30	7
40	12.26	13.02	6
50	13.71	14.65	7

This increase for outward flow injection is thought to be due to the circulation of the air in the trunk in the vicinity of the nozzle plate. The circulation was such that it would enhance the outward injection flow rate and inhibit the inward injection flow rate. This condition is peculiar to the test section used and should be avoided if possible in a new apparatus.

Appendix H

Tabulated Theoretical and Experimental Data for the Flow Coefficient and Power-Height Parameter

Table VI a. Theoretical and Experimental Values of the
Flow Coefficient and Power-Height Parameter,
Configuration 21 (Single Slot at 0 Degrees)

R	$C_{Q_{exp}}$	$C_{hd_{thy}}$	$C_{hd_{exp}}$	$\frac{C_{hd_{thy}}}{C_{hd_{exp}}}$
.003	1.000	∞	∞	—
.111	0.963	1.560	2.640	.591
.178	0.963	1.231	1.877	.656
.204	0.932	1.187	2.506	.474
.245	0.917	1.101	2.639	.417
.304	0.874	1.038	2.794	.372
.349	0.853	0.992	2.927	.339
.407	0.806	0.973	2.803	.347
.459	0.785	0.940	2.698	.348
.504	0.749	0.941	2.704	.348
.568	0.716	0.927	2.694	.344
.609	0.674	0.951	2.581	.368
.646	0.647	0.962	2.817	.341

Table VI b. Theoretical and Experimental Values of the
Flow Coefficient and Power-Height Parameter,
Configuration 22 (Single Slot at 30 Degrees)

R	$C_{Q_{exp}}$	$C_{hd_{thy}}$	$C_{hd_{exp}}$	$\frac{C_{hd_{thy}}}{C_{hd_{exp}}}$
.006	1.000	∞	∞	—
.105	0.968	1.061	1.612	.658
.151	0.941	0.912	1.455	.627
.200	0.889	0.839	1.481	.563
.252	0.884	0.751	1.501	.500
.298	0.837	0.730	1.530	.476
.345	0.822	0.690	1.641	.420
.415	0.776	0.667	1.824	.366
.444	0.767	0.652	1.956	.333
.505	0.729	0.644	2.259	.285
.538	0.707	0.642	2.329	.227

Table VI c. Theoretical and Experimental Values of the
Flow Coefficient and Power-Height Parameter,
Configuration 23 (Single Slot at 60 Degrees)

R	$C_{Q_{exp}}$	$C_{hd_{thy}}$	$C_{hd_{exp}}$	$\frac{C_{hd_{thy}}}{C_{hd_{exp}}}$
.017	1.000	∞	∞	—
.106	1.013	0.823	1.987	.414
.146	1.025	0.702	1.535	.457
.204	1.007	0.594	1.248	.476
.253	0.908	0.587	1.121	.524
.306	0.847	0.572	1.074	.533
.348	0.837	0.543	1.040	.522
.399	0.788	0.538	0.996	.540
.445	0.778	0.516	1.000	.516
.500	0.732	0.518	0.960	.540
.548	0.724	0.500	0.982	.509
.601	0.691	0.500	0.991	.505
.651	0.669	0.496	1.019	.487
.648	0.625	0.513	1.042	.492

Table VI d. Theoretical and Experimental Values of the
Flow Coefficient and Power-Height Parameter,
Configuration 24 (192 Holes at 0 Degrees)

R	$C_{Q_{exp}}$	$C_{hd_{thy}}$	$C_{hd_{exp}}$	$\frac{C_{hd_{thy}}}{C_{hd_{exp}}}$
.000	1.000	∞	∞	—
.101	0.969	1.627	7.757	.210
.162	0.966	1.286	5.300	.243
.211	0.953	1.143	4.037	.283
.263	0.944	1.032	3.425	.301
.301	0.932	0.977	2.934	.333
.369	0.907	0.908	2.562	.354
.401	0.893	0.885	2.279	.388
.453	0.871	0.853	2.158	.395
.514	0.846	0.824	1.858	.443
.564	0.812	0.820	1.769	.464
.603	0.793	0.812	1.608	.505
.662	0.757	0.812	1.494	.544
.691	0.741	0.811	1.403	.578
.762	0.675	0.844	1.280	.659
.813	0.646	0.859	1.170	.734
.861	0.592	0.911	1.142	.798
.900	0.542	0.972	1.061	.916

Table VI e. Theoretical and Experimental Values of the
Flow Coefficient and Power-Height Parameters
Configuration 25 (192 Holes at 30 Degrees)

R	$C_{Q_{exp}}$	$C_{hd_{thy}}$	$C_{hd_{exp}}$	$\frac{C_{hd_{thy}}}{C_{hd_{exp}}}$
				$C_{hd_{exp}}$
.017	1.000	∞	∞	—
.121	1.012	1.023	2.891	.354
.160	0.917	0.908	2.592	.350
.212	0.895	0.809	2.179	.371
.272	0.873	0.732	1.851	.395
.313	0.854	0.698	1.743	.400
.366	0.832	0.663	1.572	.422
.421	0.803	0.640	1.471	.435
.461	0.783	0.627	1.367	.459
.510	0.760	0.614	1.314	.467
.565	0.727	0.610	1.194	.511
.617	0.695	0.611	1.182	.517
.663	0.670	0.611	1.115	.548
.710	0.638	0.620	1.077	.576
.743	0.613	0.601	1.053	.599
.808	0.561	0.661	0.988	.669
.865	0.513	0.698	0.941	.742
.909	0.462	0.756	0.917	.824

Table VI f. Theoretical and Experimental Values of the
Flow Coefficient and Power-Height Parameter,
Configuration 26 (192 Holes at 60 Degrees)

R	$C_{Q_{exp}}$	$C_{hd_{thy}}$	$C_{hd_{exp}}$	$\frac{C_{hd_{thy}}}{C_{hd_{exp}}}$
.050	1.000	∞	∞	--
.110	0.949	0.853	2.222	.384
.157	0.934	0.723	1.926	.375
.209	0.908	0.645	1.620	.398
.272	0.881	0.583	1.379	.423
.306	0.864	0.560	1.321	.424
.351	0.839	0.539	1.226	.440
.406	0.814	0.517	1.151	.449
.455	0.790	0.503	1.119	.450
.501	0.764	0.496	1.068	.464
.558	0.732	0.490	1.033	.474
.608	0.704	0.488	0.985	.495
.671	0.669	0.489	0.978	.500
.722	0.628	0.502	0.936	.536
.757	0.608	0.507	0.913	.555
.798	0.567	0.529	0.905	.585
.854	0.514	0.564	0.860	.656
.898	0.468	0.603	0.862	.670

Table VI g. Theoretical and Experimental Values of the
Flow Coefficient and Power-Height Parameter,
Configuration 27 (Four Slots at 0 Degrees)

R	$C_{Q_{exp}}$	$C_{hd_{thy}}$	$C_{hd_{thy}}$	$\frac{C_{hd_{thy}}}{C_{hd_{exp}}}$
.000	1.000	∞	∞	—
.111	0.946	1.586	4.612	.344
.166	0.922	1.329	3.406	.390
.217	0.908	1.182	3.144	.376
.255	0.897	1.103	2.874	.384
.306	0.873	1.035	2.588	.400
.351	0.856	0.987	2.478	.398
.396	0.830	0.957	2.128	.450
.463	0.796	0.923	1.918	.481
.501	0.774	0.913	1.758	.519
.569	0.733	0.904	1.645	.550
.607	0.708	0.906	1.485	.610
.670	0.664	0.920	1.417	.649
.704	0.640	0.931	1.317	.707
.801	0.551	1.014	1.182	.858
.846	0.502	1.082	1.119	.967
.894	0.454	1.164	1.061	1.097

Table VI h. Theoretical and Experimental Values of the
Flow Coefficient and Power-Height Parameter,
Configuration 28 (Four Slots at 30 Degrees)

R	$C_{Q_{exp}}$	$C_{hd_{thy}}$	$C_{hd_{exp}}$	$\frac{C_{hd_{thy}}}{C_{hd_{exp}}}$
.038	0.999	∞	∞	—
.114	0.975	1.013	2.241	.452
.159	0.954	0.875	1.809	.484
.216	0.923	0.778	1.402	.555
.271	0.906	0.706	1.220	.579
.307	0.892	0.674	1.198	.563
.357	0.866	0.644	1.116	.577
.401	0.845	0.623	1.167	.534
.456	0.817	0.605	1.124	.538
.501	0.787	0.599	1.107	.541
.567	0.747	0.592	1.070	.553
.606	0.718	0.597	1.091	.547
.664	0.680	0.602	1.069	.563
.701	0.645	0.618	1.066	.580
.761	0.595	0.642	1.018	.631
.801	0.554	0.672	1.033	.651
.848	0.509	0.710	0.982	.723
.904	0.442	0.793	0.962	.824

Table VI 1. Theoretical and Experimental Values of the
Flow Coefficient and Power-Weight Parameter,
Configuration 29 (Four Slots at 60 Degrees)

R	$C_{Q_{exp}}$	$C_{hd_{thy}}$	$C_{hd_{exp}}$	$\frac{C_{hd_{thy}}}{C_{hd_{exp}}}$
.047	0.997	∞	∞	—
.110	0.990	0.818	2.328	.351
.142	0.985	0.724	1.779	.407
.207	0.967	0.609	1.463	.416
.261	0.962	0.545	1.304	.418
.300	0.950	0.515	1.220	.422
.356	0.939	0.478	1.120	.427
.412	0.916	0.456	1.061	.430
.455	0.906	0.438	1.023	.428
.504	0.879	0.429	0.994	.432
.569	0.846	0.420	0.926	.454
.600	0.817	0.424	0.959	.442
.668	0.769	0.426	0.923	.462
.706	0.727	0.439	0.942	.466
.749	0.693	0.446	0.932	.479
.796	0.639	0.470	0.886	.530
.864	0.543	0.531	0.941	.564
.905	0.488	0.577	0.960	.601